Enhanced trace element mobilization by Earth's ice sheets

Jon R. Hawkings[1,2*], Mark L. Skidmore[3], Jemma L. Wadham[4], John C. Priscu[5], Peter L. Morton[1], Jade E. Hatton[6], Christopher B. Gardner[7], Tyler J. Kohler[8], Marek Stibal[9], Elizabeth A. Bagshaw[10], August Steigmeyer[3], Joel Barker[11], John E. Dore[5], W. Berry Lyons[7], Martyn Tranter[4], Robert G. M. Spencer[1] and the SALSA Science Team

[1] *National High Magnetic Field Laboratory Geochemistry Group and Department of Earth, Ocean and Atmospheric Sciences, Florida State University, USA*

[2] *German Research Centre for Geosciences GFZ, Potsdam, Germany*

[3] *Department of Earth Sciences, Montana State University, USA*

[4] *School of Geographical Sciences, University of Bristol, UK*

[5] *Department of Land Resources and Environmental Sciences, Montana State University, USA*

[6] *School of Earth Sciences, University of Bristol, UK*

[7] *School of Earth Sciences, Byrd Polar and Climate Research Center, The Ohio State University, USA*

[8] *Stream Biofilm and Ecosystem Research Laboratory, School of Architecture, Civil and Environmental Engineering, École Polytechnique Fédérale de Lausanne, Lausanne, Switzerland*

[9] *Department of Ecology, Faculty of Science, Charles University, Prague, Czechia*

[10] *School of Earth and Ocean Sciences, Cardiff University, Main Building, Park Place, Cardiff, UK*

[11] *Department of Earth and Environmental Sciences, University of Minnesota, USA*

***** Corresponding author Dr. Jon R. Hawkings (jhawkings@fsu.edu).

Classification: Physical Sciences; Earth, Atmospheric and Planetary Sciences

Abstract

Trace elements sustain biological productivity, yet the significance of trace element mobilization and export in subglacial runoff from ice sheets is poorly constrained at present. Here we present size-fractionated (0.02, 0.22 and 0.45 μm) concentrations of trace elements in subglacial waters from the Greenland Ice Sheet (GrIS) and the Antarctic Ice Sheet (AIS). Concentrations of immobile trace elements (e.g., Al, Fe, Ti) far exceed global riverine and open ocean mean values and highlight the importance of subglacial aluminosilicate mineral weathering and lack of retention of these species in sediments. Concentrations are higher from the AIS than the GrIS, highlighting the geochemical consequences of prolonged water residence times and hydrological isolation that characterize the former. The enrichment of trace elements (e.g., Co, Fe, Mn and Zn) in subglacial meltwaters compared to seawater and typical riverine systems, together with the likely sensitivity to future ice sheet melting, suggests that their export in glacial runoff is likely to be important for biological productivity. For example, our dissolved Fe concentration (20,900 nM) and associated flux values (1.4 Gmol $year^{-1}$) from AIS to the Fe-deplete Southern Ocean exceed most previous estimates by an order of magnitude. The ultimate fate of these micronutrients will depend on the reactivity of the dominant colloidal size fraction (likely controlled by nanoparticulate Al and Fe (oxyhydr)oxide minerals) and estuarine processing. We contend that ice sheets create highly geochemically reactive particulates in subglacial environments, which play a key role in trace elemental cycles, with potentially important consequences for global carbon cycling.

Significance statement

Trace elements are integral to biogeochemical processes at the Earth's surface and play an important role in the carbon cycle as micronutrients to support biological productivity. We present new data from the Greenland and Antarctic ice sheets to demonstrate the importance of subglacial biogeochemical processes in mobilizing substantial quantities of these elements. Usually immobile elements are found in subglacial meltwaters at elevated concentrations compared to typical rivers, with most exhibiting distinctive size fractionation due to adsorption onto nanoparticles. Our findings suggest that ice sheets need to be included in models of global biogeochemical cycles of trace elements and studies of the fertilization of adjacent marine systems, especially the Southern Ocean, due to large export fluxes of micronutrients, most notably iron.

1. Introduction

Ice sheets cover almost 10 % of Earth's land surface area at present, up to 30 % during the last glacial maximum, and account for ~ 99 % of land ice mass, yet relatively little is known about the biogeochemical conditions beneath them and their importance in polar biogeochemical cycles (1). Both the Greenland Ice Sheet and Antarctic Ice Sheet (GrIS and AIS respectively) are undergoing rapid change due to the disproportionate impact of climatic warming in the polar regions, with annual runoff and solid ice discharge contributing ~ 1 mm of sea level rise equivalent per year over the last decade (2, 3). Extensive subglacial hydrological networks exist beneath both ice sheets, including saturated sediments, distributed and channelized water flow paths ("rivers" under ice), and interconnected subglacial lakes that drain into the ocean (4-8). These subglacial hydrological systems support elevated rates of biogeochemical weathering relative to global riverine values (9, 10). High elemental yields from glacial catchments are thought to be sustained by an abundant supply of highly reactive comminuted rock flour with reactive mineral surfaces, produced from high physical erosion rates and elevated rock:water ratios at the ice-rock/sediment interface (11, 12).

Ice sheet subglacial meltwaters have recently been identified as important sources of reactive sediment, solute and nutrients to downstream ecosystems (13-16), highlighting a potentially important, yet poorly understood contribution to global carbon cycling (1). The majority of samples have been collected from comparatively accessible glacial field sites, with extremely limited data available from Antarctic subglacial environments due to extreme technological and logistical challenges of access (17, 18). Given the paucity of data, we do not understand the

implications of changing ice sheet melt for biogeochemical cycling in the polar regions, and their impact on local and regional processes (19).

Trace element (TE; elements present at low "dissolved" concentrations in natural waters, operationally usually < 50 ppb) concentrations in glacial meltwaters have received minor attention to date (15, 20, 21). The concentration and speciation of TEs may provide important information about the chemical weathering environment, redox processes, water sources, and subglacial hydrological pathways that are not always apparent using only major ion chemistry (22-24), although the source, speciation, transformation and co-association of many trace elements are still not well understood. For example, Al and V (and to a lesser degree Ba) can be used as tracers of silicate weathering intensity (25), Mo, Cd and Zn are strongly chalcophilic elements and their presence is indicative of oxidation of sulfide minerals (26, 27), and Fe and Mn are redox sensitive and therefore their presence and speciation indicate reducing source waters and elucidates oxidation rates (28). A number of TEs (e.g. Ni, Co, Pb and Cr) are siderophiles and therefore their mobility can provide information of weathering, transport and form of Fe, and, by association, biologically mediated redox processes (29). U can be used as a tracer of oxidative weathering and is sourced mainly from sedimentary rocks (30), while Sr concentrations can be an excellent indicator of carbonate mineral weathering (31). Furthermore, many TEs are biologically essential micronutrients that play critical roles in cellular processes, including C, N and P transport and assimilation, and as components of metabolic co-enzymes/metalloproteins (e.g., Fe, Mn, Mo, Co, Zn, Cu, Cd, Mo, V; (32-34)). Consequently their export from ice sheets to downstream ecosystems can have important implications for biological productivity and associated patterns of nutrient limitation and elemental inventories (15, 35, 36).

We hypothesize that ice sheets play an important yet poorly constrained role in TE cycling given the elevated chemical erosion rates under large ice masses (9, 37, 38), the unique biogeochemical weathering environment (Table S1) in subglacial hydrological systems and the large and increasing ice sheet freshwater export. Constraining TE export from ice sheets is critical for understanding downstream elemental cycling and associated ecosystem response, and the implications of future changes to glacial meltwater discharge.

We present size-fractionated TE concentration data (< 0.02 μm, "soluble", s[element]; < 0.45, "dissolved", d[element]; 0.02 - 0.45μm, "colloidal/nanoparticulate", cn[element]) for subglacial meltwaters sampled beneath the Antarctic (Mercer Subglacial Lake; SLM; a hydrologically-active subglacial lake) and emerging from the Greenland (Leverett Glacier; LG; a large ice sheet catchment) ice sheets (Fig. 1). We use these data to (i) examine how biogeochemical weathering processes and water sources influence the TE geochemistry of the subglacial environment and infer the potential significance of glacially derived TEs to downstream ecosystems surrounding ice sheets, (ii) determine the magnitude of colloidal/nanoparticulate phases for the majority of TEs measured, and (iii) assess the enrichment/depletion of micronutrients in glacial meltwaters compared to global non-glacial riverine mean values (hereafter referred to as "riverine mean values") and typical seawater concentrations. Our results significantly advance the understanding of biogeochemical processes beneath large ice sheets and highlight the potential importance of meltwaters in global TE inventories.

2. Results and discussion

2.1 Controls on trace element composition of AIS and GrIS meltwaters

Elemental concentrations in SLM and LG waters span an extremely large range with clear patterns of size fractionation in the "dissolved" <0.45 μm phase (dTE; Figs. 2 and 3, Table S1). Data from both locations indicate that the dominant dTE in subglacial meltwaters are those typically associated with lithogenic weathering of the more abundant elements in the Earth's crust and oxyhydroxide mineral phases, i.e., dAl, dFe and dTi, with concentrations higher than the mean of non-glacial rivers (Fig. 2b, Table S1). For example, dFe concentrations in LG and SLM were up to an order of magnitude higher than mean riverine waters (2,390 and 20,900 nM compared to 1,180 nM), dTi concentrations were at least one order of magnitude higher (277 and 2,080 nM in LG and SLM waters respectively, compared to ~10 nM riverine mean), and dAl concentrations at LG and SLM (351 – 105,000 nM) are similar only to concentrations reported in GrIS meltwaters (300 – 13,600 nM, (21)). The elevated concentrations of typically less mobile elements point to the influence of biogeochemical weathering processes in waters with a high pH (up to 9.6 at LG and 8.2 at SLM; Table S1). The high concentrations of these elements also reflect the importance of physical weathering processes generating an abundant supply of microparticles and predominance of refractory primary minerals and nanoparticulate (oxyhydr)oxides, as observed previously in glacial meltwaters (23, 39, 40), despite the low temperatures (~ 0 °C) commonly associated with suppressed weathering rates. These weathering processes hold even within SLM where subglacial water residence times are prolonged (~years; (41)), underlying sediments are of contrasting origin (overridden marine sediments vs freshly crushed shield bedrock), and suspended sediment concentrations are relatively low (~20 mg L^{-1} at SLM vs ~1,000 mg L^{-1} at LG), indicating lower local physical erosion rates and turbulence.

144 The predominant driver of TE composition in these subglacial systems appears to be the
145 weathering of silicate minerals, as elucidated from the abundance of TEs commonly sourced
146 from silicate weathering. For example, Vanadium (V) is almost entirely derived from silicate
147 weathering (25) and concentrations in ice sheet meltwaters exceeded the riverine mean value
148 (~14 nM) (24, 25), with LG waters more than twice as concentrated on average (dV 31.1 nM, up
149 to 89.2 nM) and SLM waters more than an order of magnitude higher (dV 265 nM; Fig. 3, Table
150 S1). This contrasts with more variable dissolved silicon (Si) concentrations, which are low in LG
151 waters (9.2 – 56.9 μM; (42)), with Si likely retained in secondary weathering products (43) while
152 V is not, yet similar to global riverine concentrations of ~158 μM in SLM (120 – 140 μM; Fig.
153 2) (44). Other trace elements typically associated with silicate weathering and at much higher
154 abundance in silicate rocks than carbonate rocks are also found at high concentrations in
155 meltwaters from both ice sheets, especially Al, Ti, Co, Cr and Ni (Fig. 2b) (45).
156
157 The major ion chemistry of Whillans Subglacial Lake (SLW) adjacent to SLM (Fig. 1; (38)), and
158 from GrIS (9, 16, 37, 42) is also consistent with enhanced silicate mineral weathering beneath ice
159 sheets (46). This contrasts older views that silicate mineral weathering was insignificant beneath
160 glacial systems as valley glaciers typically exhibit geochemical signatures of carbonate
161 weathering (9, 12). The principal weathering conditions are likely to be different at the two ice
162 sheet locations. We contend that GrIS waters exhibit silicate weathering signatures because the
163 underlying bedrock is either carbonate poor (37, 47) and/or that meltwater residence times are
164 prolonged in larger GrIS catchments (42) enhancing weathering of minerals with slower
165 dissolution kinetics. The high pH of LG meltwaters (up to 9.6) also enhances the solubility of
166 primary aluminosilicate minerals (12). AIS meltwaters exhibit geochemical conditions of waters

with long residence times and highly weathered sediments, where reactive minerals have been previously weathered from the rock matrix (38), and where porewaters in the subglacial sediments are likely to provide a concentrated source of solute to waters via diffusion (38).

Sr concentrations in LG and SLM meltwaters reinforce this interpretation. Sr is found at high concentrations in carbonate minerals, with Sr^{2+} substituting for Ca^{2+}, and is therefore common in limestones, dolostones and evaporites. Concentrations of Sr in LG meltwaters are low (51.6 nM; Fig. 2a, Table S1), consistent with previous measurements (47). SLM Sr concentrations are similar to the riverine mean (~850 nM vs 600 – 900 nM; Figs. 2 and 3; (31)) but much lower than riverine catchments where carbonate/evaporitic weathering dominates (e.g., the Colorado River, ~10,000 nM, Rhone and Rhine River's, ~ 6,000 nM, and the Mekong River, ~ 3,000 nM; (31)).

Weathering of sulfide minerals also appears to contribute to meltwater TE composition (38). High cnFe and SO_4 concentrations in all samples indicate iron sulfide oxidation may be an important weathering pathway for generation of Fe oxyhydroxide nanoparticle aggregates 0.02-0.45 μm in size (Fig. 2) (23, 48). The importance of sulfide mineral weathering is reinforced from Mo, a strongly chalcophilic element preferentially weathered from sulfide minerals (predominantly pyrite; (26)). Mo concentrations in LG (1.9 – 11.3 nM) are similar to the global riverine mean (8 nM; (26)) and are substantially higher in SLM (52.9 nM; Figs. 2 and 3).

2.2 The colloidal world of subglacial environments

189 At least 14 of the 17 elements measured have a colloidal/nanoparticulate (cn) component in
190 glacial meltwaters (Table S1, Fig. 3). TEs can be broadly separated into three operationally
191 defined classifications (Fig. 3): (Group 1) those strongly associated with the cn phase (>75% cn);
192 (Group 2) those moderately associated with the cn phase, but with a significant soluble fraction
193 (≥25% but ≤75% cn); and (Group 3) elements predominantly associated with the soluble phase
194 (<25% cn). SLM and LG meltwaters share nine common Group 1 elements: Ti, Fe, Pb, Co, Ni,
195 Ba, Al, Zn and Cu; two common Group 2 elements: Cd and V; and three common Group 3
196 elements: Li, Sr and Mo. Cr is found mainly in the colloidal phase at both locations but in Group
197 1 for LG and Group 2 for SLM. U and Mn have contrasting distributions; U is in Group 1 for LG
198 and Group 3 for SLM, while Mn is a Group 1 element at SLM only found in colloidal size
199 fractions, compared to Group 2 at LG, with a substantial proportion (>33%) present as sMn.
200
201 Most elements fall into Group 1 in both ice sheet environments (Fig. 3). This phase is likely to
202 consist mostly of inorganic material since dissolved organic carbon (DOC) concentrations are
203 very low at both SLM and LG sampling locations (~ 30 μM, Table S1; (49)). The large
204 concentrations and proportions of Fe and Al in the cn size fraction (cnFe = 2,390 nM at LG and
205 20,900 nM at SLM; cnAl = 14,200 nM at LG and 65,000 nM at SLM, Fig. 2 and 3) indicate that
206 Fe oxyhydroxide nanoparticles (likely ferrihydrite, goethite and hematite) and Al oxyhydroxide
207 nanoparticles (likely poorly crystalline alumina or gibbsite) control the speciation of these
208 elements via their large adsorption capacity, surface precipitation or coprecipitation (50).
209 Elements that have an affinity with oxyhydroxide minerals (e.g., Cr, Co, Zn, Ni, Pb via binding
210 to -OH functional groups; (29, 51)), especially just below the oxyhydroxide zero point of charge
211 (pH ~9 for Fe oxyhydroxides), are present at much lower concentrations in the soluble phase

(<20 % of dTE; Fig. 3). A large sorption capacity of colloidal material for other trace elements is also observed in large non-glacial riverine systems, although not to the same degree (51).

The unique features of subglacial weathering environments provide an explanation for the predominance of these colloidal/nanoparticulate TE phases. The low temperatures (~ 0 °C) may aid in slowing the aggregation and aging of nanoparticles into denser, larger size fractions >0.45 μm in size, with smaller aggregates having a greater adsorption capacity due to their extremely high surface area to volume ratios (52). Additionally, aggregation under higher pH conditions (mean pH was >8, up to 9.6; Table S1) has been found to generate less ordered porous aggregates with high sorption properties (53).

It is possible that other mechanisms inducing this size fractionation are important. Nanoclays rich in Al and Fe (e.g., allophane) can also adsorb/incorporate less abundant elements (54). Alternatively, the extremely fine size fraction of comminuted sediments allow crushed primary rock material to pass through larger pore size filter membranes (55), and thus this phase is more indicative of a weathered bulk bedrock signature (i.e., mobile elements have been leached, leaving relatively immobile elements). It is likely this process would differ for SLM (long residence time) versus LG (comparatively short residence time), with aged secondary minerals (e.g., nanoclays) dominating in the former and primary minerals, or freshly precipitated secondary minerals (e.g., amorphous iron oxyhydroxides) dominating in the latter.

The consideration of the cn size fractions appears to be critical in determining the behavior and concentration of filterable TEs in subglacial meltwaters. For example, the operationally defined

filter membrane pore size cut off has a substantial impact on the observed concentration of TEs in SLM (Fig. 3). In addition to 0.02 and 0.45 μm, 0.22 μm filtered samples were taken from SLM allowing partitioning between small (0.02 - 0.22 μm; cn^{small}) and large (0.22 - 0.45 μm; cn^{large}) cn species. These data show that colloidal/nanoparticulate phases were more abundant in the larger size fraction. In particular, < 10 % of cnTi and cnFe is contained in the cn^{small} phase compared to > 90 % in the cn^{large} phase. The geomicrobiological implications of this partitioning are uncertain as the reactivity of this material is not well understood. Given the very high surface area to volume ratios of these particles, we hypothesize they are highly reactive but likely require more complex and energy intensive processing before biological uptake. The large difference in concentration between colloidal size fractions likely reflects the aggregation of nanoparticulate material to features >0.2 μm, as observed in high resolution photomicrographs of glacial suspended sediments (23, 39).

2.3 Contrasting trace element cycling under ice sheets

Several broad similarities exist in the TE composition of SLM and LG meltwaters despite the contrasting hydrological, geological and geochemical conditions. Most TEs appear to have a colloidal/nanoparticulate component, as discussed above. Only Sr, Mo and Li existed predominantly in the soluble phase in both environments likely because they are highly mobile elements (particularly Sr and Mo) with geochemical behavior similar to other alkaline and alkaline-earth cations (Fig. 3 and 4). Additionally, the presence of sMo at similar or elevated concentrations to riverine waters at both field sites also implies contributions from an oxic weathering environment (likely alongside flushing of hypoxic/anoxic stored waters under LG) (26), which is reinforced by mean dissolved O_2 saturation exceeding 100 % (with respect to

atmospheric O_2) at both sampling sites (Table S1; (56)). Subglacial concentrations of dissolved lithogenic TEs associated with the most abundant crustal elements are also high in both meltwaters, as previously discussed.

Several key differences exist between the subglacial meltwaters sampled despite these broad similarities. The major difference between subglacial meltwaters in SLM and emerging from LG is the absolute elemental concentration. Both cnTE and sTE concentrations in SLM meltwaters are generally much higher than in LG meltwaters (up to an order of magnitude; Table S1, Fig. 2c). High concentrations of dTE in AIS subglacial environments have been hypothesized (57) given the long residence time of AIS meltwaters, inputs of solute from underlying sediments (38), no subglacial meltwater dilution from surface meltwater (as with the GrIS)(13, 42), and elevated macronutrient concentrations in SLW (15), but has been supported by little evidence until now. Contrasting hydrological environments are also reflected in the mean specific conductance of meltwaters (a proxy for solute concentration), which differ by more than an order of magnitude (12.6 vs 272 $\mu S\ cm^{-1}$; Table S1), as well as differences in major ion composition (9, 38, 42). These differences also highlight the distinct biogeochemical processes occurring beneath ice sheets. Enhanced silicate weathering in long residence time AIS meltwaters produces an abundance of clay minerals and the potential for surficial ion exchange on these clay minerals in long residence time AIS meltwaters (38). This contrasts with shorter residence times of GrIS meltwaters with rapid silicate hydrolysis and carbonation reactions on freshly crushed primary rock minerals (42), and substantial dilution by incoming fresh supraglacial meltwaters.

280 The speciation of two trace elements highlights some of the variation between ice sheet
281 environments: U (100 % sU in AIS, but < 1 % sU in GrIS) and Mn (< 1 % sMn in AIS, but > 35
282 % sMn in GrIS). This contrasting behavior is somewhat surprising given the broad similarities
283 observed between other TEs. The behavior of U may relate to the sediment source, with SLM
284 underlain by overridden marine sediments (with U commonly enriched in sedimentary
285 environments (30)), versus LG sediments generated from the Precambrian shield silicate
286 bedrock, likely to be depleted in U (24, 30). SLM waters are also highly enriched in U compared
287 to mean riverine values (29.7 nM vs 0.78 nM; (30); Table S1). Predominance of cnU phases in
288 LG meltwaters may be linked to adsorption onto nanoparticulate Fe oxyhydroxides (58).
289 Evidence of this is given by the lower cnFe:cnU ratio, < 5,000, relative to the Fe:U upper
290 continental crust ratio of shield bedrock, ~ 15,000 (45). No U is associated with the cn fraction at
291 SLM, possibly due to stabilization by ligands (e.g., as $[UO_2(CO_3)_3]^{4-}$ (59)) or reflecting the
292 contrasting transport processes (likely grinding of primary rock particles and turbulent water
293 flow at LG versus diffusion from sediments in SLM).
294
295 The absence of sMn in SLM waters versus LG meltwaters is likely indicative of the longer water
296 residence times (~years; (41)) combined with oxidative weathering environment (>100 % O_2
297 saturation with respect to atmospheric O_2; Table S1). The lack of sMn in SLM waters indicates
298 almost complete oxidation of soluble Mn^{2+} species to insoluble $Mn^{3+/4+}$, and/or adsorption of
299 Mn^{2+} to Mn oxyhydroxides or clays (60). Conversely, in GrIS catchments meltwater transport
300 times through the subglacial drainage systems to the meltwater portal are comparatively rapid
301 (hours to weeks (61)). Furthermore, isolated hypoxic and anoxic subglacial environments present
302 underneath the GrIS (62) are favorable for generating high point concentrations of sMn (via Mn

303 reduction) and allow persistence of Mn^{2+} despite meltwater being fully oxygenated upon
304 sampling. The half-life of Mn^{2+} in oxygenated waters, before oxidation to Mn^{3+}/Mn^{4+} and
305 precipitation as Mn oxides, is significantly longer than Fe^{2+} in the absence of stabilizing ligands
306 (hours to weeks versus seconds to minutes (63)), especially at low temperatures, and it appears
307 soluble Mn^{2+} species persist during transport in the LG subglacial system where stored
308 anoxic/hypoxic subglacial waters are mixed with oxygenated surface meltwater.
309
310 TE mobility can also help explain differences between SLM (AIS) and LG (GrIS) chemical
311 weathering environments. Elemental mobility was estimated via a first order approach (22) by
312 normalization of dissolved concentrations to mean upper continental crust composition (45) and
313 then normalizing to the resulting Na rock:solution ratio so that Na = 1 ("mobility index" - MI).
314 Our data indicate comparatively low mobility of TE in SLM meltwaters versus relatively high
315 mobility in LG meltwaters compared to non-glacial rivers (Fig. 4). Highly chemically weathered
316 "bleached" sediments underlie SLM, with less mobile elements (MI <1; Fig. 4b) more likely
317 incorporated into secondary weathering products, likely clay minerals >0.45 μm in size via
318 adsorption/ion exchange and/or co-precipitation (38, 64), with highly mobile elements (MI >1;
319 Figure 4a) retained in solution. In contrast, typically less mobile elements (MI < 1) generally
320 have higher mobility in LG meltwaters than both SLM and mean riverine waters, likely
321 reflecting hydrolysis of primary rock minerals after comminution (42).
322
323 Finally, LG meltwaters exhibit large variability in TE concentrations driven by seasonal changes
324 in the subglacial drainage system in response to surface meltwater forcing (42, 61, 65). It is
325 currently unknown if there is substantial temporal variation in meltwater composition in SLM or

under AIS more widely. Any TE geochemical variability in SLM would be likely to reflect drain/refill cycles in the lake (41), the geochemical consequences of which are unknown but unlikely to be as large as the variation observed in meltwater emerging from LG, given the significant seasonal hydrochemical evolution of GrIS catchments (42).

2.4 Implications for downstream biogeochemical cycling

Several TE are essential micronutrients for microbiota, serving as important components of (co-) enzymes and performing essential roles in cellular processes such as nitrogen and carbon fixation (32). The most important trace elements for microbial metabolism are thought to be Fe, Mn, Mo, Co, Zn, Cu, Ni, V and Cd (32, 33), several of which are can be limiting or co-limiting for photoautotrophic and heterotrophic activity in marine (35, 66) and freshwater ecosystems (36). Recently, ice sheets have been hypothesized to be significant sources of Fe to the ocean, with high concentrations of dFe found in meltwaters from the GrIS (23, 48, 67, 68) and (sub)Antarctic maritime islands (69, 70), as well as significant quantities of labile particulate Fe rafted in icebergs (71, 72). Limited data exists for glaciated environments, apart from spot samples from several Greenlandic glaciers (21) that alluded to high concentrations in meltwater. The two ice sheets deliver >2000 km^3 of freshwater (i.e., >5 % of the riverine freshwater flux (73)) to the ocean each year and this is increasing. Therefore, a first order consideration of the associated TE input is important in understanding any influence on biological productivity in polar waters adjacent to the ice sheets and potential nutrient limitation/alleviation. Our discussion focuses on flux estimates “at the gate” where meltwater enters the marine environment (Tables 2 and 3), but we acknowledge that estuarine processing can drastically modulate the TE flux into the open ocean (74, 75).

Nearly all dissolved micronutrient concentrations are elevated in glacial meltwaters from the GrIS and AIS relative to mean ocean concentrations (Table S1). This contrasts with the relatively low dissolved macronutrient (C, N and P) concentrations reported previously for GrIS (76, 77), but is consistent with higher concentrations reported beneath AIS (Fig. 2a (15)). A notable exception is Cd, which is lower in both GrIS (0.015 ± 0.019 nM) and AIS (0.21 ± 0.011 nM) meltwaters comparative to non-glacial riverine waters (0.712 nM, (22)) and bulk oceanic waters (0.6 nM, (78)). Cd is a highly mobile but rare chalcophilic element, so these low concentrations indicate Cd-bearing sulfides (e.g., zinc sulfides rich in Cd such as sphalerite and cadmium sulfides such as greenockite) are depleted in sediments underlying LG and SLM, or reflects an anthropogenic source of the high dCd in rivers (27), which is absent in pristine glacial systems. SLM waters are enriched in all other bioessential trace elements with concentrations of dCo, dCu, dFe, dMn and dZn all more than one order of magnitude higher in SLM waters than marine waters and typically exceed or are similar to mean riverine concentrations (Table S1; Fig. 2). LG concentrations also exceed bulk oceanic concentrations and are broadly similar to mean riverine concentrations (Table S1; Fig. 2). LG Mn concentrations appear an order of magnitude lower than riverine concentrations, although they exceed bulk oceanic concentrations by more than two orders of magnitude (72.6 vs 0.3 nM; Table S1). Mean riverine Mn concentrations reported also appear biased by a lack of high quality riverine data and concentration estimates in the Amazon River (which has a disproportionate effect on the mean concentration) that span an order of magnitude (60 – 920 nM (22)). Moreover, LG dMn concentrations are similar to or exceed many North American rivers (e.g., the Columbia River, ~10-100 nM, and the Mississippi, ~1-70 nM; (28, 79)).

372

373 The relatively high "dissolved" micronutrient concentrations in ice sheet meltwaters that we
374 measured provide the first evidence that ice sheet meltwaters could supply a suite of dissolved
375 micronutrients to support biological production in coastal regions surrounding AIS and GrIS (80,
376 81). Collectively these large regional ice sheet micronutrient inputs should be considered in
377 future TE biogeochemical models where they are currently absent (66, 82, 83).

378

379 **2.5 Antarctic Ice Sheet fertilization of the Southern Ocean?**

380 Our data have particularly important implications for our understanding of ice sheet fertilization
381 of the Fe-deplete Southern Ocean (84). No size speciated dTE data from subglacial hydrological
382 systems beneath AIS have been previously obtained, although the enrichment of Fe in AIS
383 meltwaters compared to surrounding oceanic environments has been hypothesized and
384 previously measured at SLW (15, 23, 57, 68). The data we present indicate that meltwater
385 discharge from interconnected subglacial lake hydrological systems draining AIS into coastal
386 embayments is likely to elevate labile Fe concentrations (Fig. 2), supporting previously
387 hypothesized glacial Fe fertilization in coastal regions of the Southern Ocean (68-70, 85, 86).
388 The cnFe concentrations in SLM (20,900 nM) far exceed concentrations in LG and other GrIS
389 meltwaters (50 – 7,500 nM; Table S1; (48, 67)). AIS dFe flux estimates based on SLM
390 concentrations (0.66 – 2.1 Gmol year^{-1}; Table 1) exceed previous AIS estimates by an order of
391 magnitude (0.02 – 0.32 Gmol year^{-1}; (23, 69)) and are similar to GrIS dFe export estimates
392 despite the much lower discharge. The SLM values are also consistent with upper end AIS
393 subglacial meltwater Fe concentration estimates used in a study (30,000 nM; (87)), which
394 produced modeled data of Southern Ocean Fe and primary productivity consistent with

observations. Even if estuarine removal in the Siple Coast underneath the Ross Ice Shelf filters 99% of subglacially exported Fe, there is still potential for significant AIS Fe fertilization of coastal ecosystems if these species persist and are labile. A more recent modelling study found limited, more localized fertilization potential of ice shelf meltwater (88), highlighting the complexities of evaluating ice sheet influence on downstream productivity. However, the mechanisms of Fe delivery discussed in that study differ (ice shelf melt versus subglacial meltwater discharge), meltwater concentrations used were lower, and it remains difficult to disentangle meltwater (direct and indirect) vs sediment sources (argued by the authors to be more important) in coastal regions where primary productivity is high. Additional field data and biogeochemical modelling are clearly needed to disentangle and constrain the major sources of Fe to the Southern Ocean, and the impact of direct (meltwater outflow) vs indirect (glaciogenic sediments comprised in part from material deposited by meltwaters) glacial inputs.

An interesting juxtaposition exists when comparing Fe data from SLM to SLW, where the only comparative concentration estimates for the AIS exist. The dFe concentrations reported for SLW (15) are ~30 nM, compared to the phase size equivalent (<0.22 μm) measured in SLM of 981 nM. This leads to substantial variability in estimated dFe fluxes to the Siple Coast: 61 kmol year^{-1} (15), compared to 40,000 kmol year^{-1} (Table S2). The Fe export calculated from SLW was estimated to be able to maintain measured microbial activity in the Siple Coast region (based on elemental stoichiometry (15)), therefore estimates based on SLM concentrations vastly exceed that. Although filter type and pore size are not directly comparable, these differences point to the possibility of substantial spatial or temporal heterogeneity (e.g., fill/drain cycles (41)) in Fe concentrations beneath AIS and/or the influence of filtration artifacts such as membrane clogging

418 and reduction in effective pore size (89). Modeling studies of glacial Fe sources to the Southern
419 Ocean coupled to observations of euphotic zone dFe and chlorophyll *a* concentrations (87, 90)
420 and indirect observations under ice shelves (91) reveal that SLM may be more representative of
421 an enriched AIS subglacial endmember. We do not account for reactive particulate iron
422 concentrations in these estimates (e.g. amorphous ferrihydrite (39)), which were found to be
423 elevated in SLW (15) and are likely to be high in SLM. The potential for high spatial variability,
424 consistency in filtration methodology and elevated labile particulate Fe clearly demonstrate the
425 need for future coordinated studies on AIS subglacial environments.
426
427 **2.6 Modulating effects of estuarine processing**
428 The significance of subglacial trace micronutrients to downstream ecosystem processes will also
429 depend on their behavior following delivery. Downstream elemental transformations are likely to
430 be complex, with each micronutrient exhibiting unique geochemical characteristics during
431 mixing of freshwater with seawater that vary regionally, including conservative behavior (e.g.,
432 Ni, Cu, V and Mo), nonconservative excess (e.g., Mn, Co, Zn and Cd) and nonconservative
433 removal (e.g., Fe)(92). The behavior of individual elements will depend on multiple
434 biogeochemical factors such as organic matter concentration and composition, ligand binding,
435 benthic recycling (e.g., via diffusive porewater fluxes or sediment resuspension), desorption
436 from mineral surfaces, and microbial uptake or alteration (such as Mn oxidation) (79, 92). The
437 impact of micronutrients on downstream ecosystem processes will also depend on the physical
438 features of the downstream environment. Meltwaters from subglacial environments under the
439 AIS often flow into large sub-ice shelf cavities >400 km from the open ocean with long
440 residence times (several years in the Ross Ice Shelf cavity (15)). These sub-ice shelf

environments will impede immediate delivery of micronutrients to photosynthetic primary producers. Nevertheless, our results (Table 1) indicate AIS subglacial meltwaters may still be able to subsidize the micronutrient inventory in coastal regions of the Southern Ocean where high productivity has been observed, such as pelagic regions proximal to the Ross Ice Shelf downstream of Siple Coast inputs (Table S2), and other major ice streams (81). Conversely, GrIS meltwaters enter coastal regions either as turbid meltwater rivers emerging from land-terminating glaciers, or via injection into fjord at depth from tidewater glaciers. These two delivery mechanisms have been observed to drastically alter the biogeochemical conditions for primary producers and surface macronutrient concentrations, but little information is currently available on micronutrient behavior in fjords (19, 80, 93).

The presence of high colloidal TE concentrations in subglacial meltwater is likely to have significant implications for downstream transport and lability. These implications are especially important for Fe, where cnFe will aggregate, flocculate and be scavenged from the water column at low salinities, with implications for TEs associated with Fe. For example, >95% of dFe is removed in low salinity regions of Alaskan and Greenlandic estuaries/fjords, but high concentrations still remain at seawater salinities close to the coast because of the high glacial meltwater end-member concentrations (74, 75). The very high dFe concentrations observed in SLM indicate potential for long distance transport of glacially derived iron even with large removal rates. The bioavailability of colloidal species is also uncertain as they represent a complex mixture of organic and inorganic material with varying labilities. Soluble species are likely the best empirical measurement of potentially bioavailable phases, yet represent a small fraction of the total dissolved pool (Fig. 3). Colloidal species of trace metals appear more

important than soluble species in supply and removal processes in oceanic and coastal systems (94) and this will almost certainly depend on the mineralogy of the colloid/nanoparticles usually included in the filterable fraction (40).

3. Conclusions

Ice sheets export globally significant quantities of trace elements in subglacial meltwaters and as such should be considered an important component of polar biogeochemical cycling of trace elements. Trace elements in meltwaters sampled from the Greenland and Antarctic ice sheets are derived mainly from the biogeochemical weathering of silicate and sulfide minerals, consistent with previous research on major ion composition and mineralogy (9, 38, 42, 43), and further highlighting the potentially important role of ice sheets in enhanced silicate weathering and long term carbon drawdown (46). Concentrations of trace elements in subglacial meltwaters are generally high despite low temperatures, which likely reflects weathering of rock microparticles and/or long water residence times in high rock:water subglacial drainage systems. The importance of colloidal/nanoparticulate species depend on the element in question, but our data indicate a prevalence of elemental species 0.02-0.45 μm in size compared to truly soluble (<0.02 μm), aqueous species. Nanoparticulate oxyhydroxide minerals are therefore important in subglacial environments with a high sorption capacity and have important implications for lability and the ultimate fate of trace elements in the downstream cascade. The role of subglacial export of trace elements to adjacent/downstream polar ecosystems can elevate micronutrient availability and therefore the carbon cycle by sustaining or altering biological productivity. Downstream TE transport is especially relevant to Antarctica because biological productivity in the Southern Ocean surrounding the AIS is limited by Fe (84). The significance of these fluxes

will depend on sub-ice shelf and estuarine processing, which are poorly quantified at present. Our findings have implications for the understanding of elemental cycling during periods of glacial transition, including the increasingly rapid melt of the ice sheets predicted in future climate warming scenarios.

4. Methods

4.1 Study areas

4.1.1 Mercer Subglacial Lake (West Antarctic Ice Sheet)

AIS samples were collected in December 2018-January 2019 from Mercer Subglacial Lake (SLM; Fig. 1b; 84.661°S, 149.677°W) 1,092 m beneath the surface of the West Antarctic Ice Sheet. SLM is one of the largest lakes (136 km^2) beneath Siple Coast ice streams and fed by subglacial waters from the East and West Antarctic Ice Sheets. Approximately 25 % of its water is hypothesized to be sourced from beneath the East Antarctic Ice Sheet via Mercer Ice Stream (95). The lake is hydrologically active with multiple drain/fill cycles observed over the past decade (41). The lake depth was 15 m at the time of sampling and the falling ice elevation indicates the lake was in a draining stage (96). Modeling reveals that downstream flow is through subglacial channels into a marine embayment at the southern reach of the Ross Ice Shelf cavity, with episodic discharge exceeding 300 m^3 sec^{-1} during flood events (7). This region of the West Antarctic Ice Sheet is underlain by glacimarine sedimentary basins (97).

4.1.2 Leverett Glacier (Greenland Ice Sheet)

509 GrIS samples were collected from the proglacial river emerging from a subglacial portal exiting
510 Leverett Glacier (LG; 67.062°N, 50.201°W; Fig. 1a; (11, 13, 61)) in south-west Greenland
511 during the 2015 ablation season. LG is a polythermal-based glacial outlet of GrIS estimated to
512 drain a hydrologically active catchment area of ~600-900 km^2 (11), and is thought to be fairly
513 representative of GrIS land terminating catchments at large, as detailed elsewhere (13, 62). The
514 LG meltwater river feeds into a larger river system (Watson River) ~6 km downstream, which
515 discharges into Søndre Strømfjord. Bedrock geology is predominantly Precambrian Shield
516 gneiss/granite, which is the dominant geology under much of GrIS (98).
517
518 **4.2 Sample collection, processing, storage and analysis**
519 SLM water samples were retrieved using a standard 10 L Niskin bottle pre-cleaned with 1.2 M
520 HCl (followed by copious rinsing with ultra-pure water (UPW); Milli-Q; 18.2 MΩ cm^{-1}), 3 %
521 H_2O_2 and lowered through a ~0.6 m diameter borehole drilled using a microbiologically clean,
522 hot water drilling system (17, 18). A 10L Niskin bottle was retrieved in six casts into the lake
523 from 29th December 2018 to 4th January 2019. Bulk LG water runoff samples were collected by
524 hand at least once daily from 1st May to 28th July 2015 ~1 km downstream of the glacier portal to
525 capture changes in subglacial hydrology (65) as detailed below.
526
527 **4.2.1 TE sampling, processing and storage**
528 Samples for TE analysis were collected cleanly according to strict size-fractionated trace element
529 protocols ((23, 89); procedural blanks detailed in Table S3). All sampling equipment (250 mL
530 and 15 mL Nalgene® LDPE bottles, and PP/PE syringes) were cleaned sequentially in 1%
531 DECON (overnight), 6 M HCl (48 hours) and 3 M HNO_3 (48 hours), with copious rinsing in

UPW in between washes, and final drying in a laminar flow hood (ISO 5). Whatman® GD/XP PES (polyethersulfone) 0.45 µm, Millex-GP Millipore Express 0.22 µm (PES; only SLM) and Whatman® Anotop 25 0.02 µm syringe filters were cleaned with ultra-trace metal grade HCl (Optima™). The 0.22 and 0.45 µm syringe filters were cleaned by passing through 20 mL of 1.2 M HCl, with the final ~1 mL allowed to sit in the filter for ~2 hours before rinsing with 40 mL of UPW and flushing with laminar flow filtered air to dry. The 0.02 µm filters were cleaned by passing 20 mL of 0.02 M HCl, followed immediately by 20 mL of UPW and clean laminar flow filtered air to dry.

Bulk water samples were collected in 1000 mL LDPE bottles (Nalgene®), from a 10 L Niskin bottle in a field chemistry laboratory at the SLM drill site. At SLM water samples from the were decanted into a 250ml LDPE bottle inside a laminar flow hood. The laminar flow hood was lined with polyethylene sheeting, that had been wiped with 1 M HCl followed by 3 x wipes with UPW, and the sample was decanted via gravity feed through 1 M HCl rinsed silicone tubing. Approximately 1-2 L of lake water from the Niskin bottle was flushed through the tubing before collection of the TE sample. Personnel conducting the sample decanting and filtration wore full Tyvek clean room suits and polyethylene gloves. Bulk water samples at LG were collected from a fast-moving section at the side of the main proglacial river approximately 2 km downstream of the glacier portal (Fig. 1)(23) into 250 mL LDPE bottles (Nalgene®; triple rinsed with bulk sample water) zip-lock bagged and taken immediately to a designated “clean” lab tent. Filtration was performed within a lab made filtration box at LG, a large polypropylene box with one face removed and replaced with LDPE sheeting that was taped to the box in between use, thus minimizing potential contamination by dust.

555

556 Bulk samples were filtered through the 0.45 µm syringe filter (12 mL to waste/rinse, with final
557 10 mL collected), and then through a stack of 0.45 µm/0.02 µm syringe filters (12 mL to
558 waste/rinse with final 10 mL collected). Samples were additionally filtered through the 0.22 µm
559 syringe filters at SLM (12 mL to waste with final 10 mL collected). Samples were preserved in
560 the field at LG by acidifying with Optima^{TM} HNO_3 to a pH <2. Samples for TE from SLM were
561 collected from casts 1-3 and acidified with twice lab distilled ultra-trace metal grade HNO_3 ~3
562 months after collection, in a Class 100 clean lab and left acidified at room temperature for 6
563 weeks before analysis. Field blanks for LG were processed in the field with transported UPW
564 identically to samples. Niskin bottle blanks were prepared in the Crary Laboratory, McMurdo
565 Station, Antarctica, before field deployment at SLM. A 10 L Niskin was filled with UPW, left to
566 sit for ~30 minutes then processed as per samples.
567

568 A common concern with TE is contamination during sampling, especially when new sampling
569 methods are used (as at SLM). We are confident that hot water drilling introduced minimal
570 contamination at SLM. First, the water level in the borehole was reduced to lower the head
571 pressure in the borehole. Back pressuring the borehole in this manner allowed the lake water to
572 rise upward of 14 m into the borehole after breakthrough, avoiding potential contamination of
573 the lake by drill water entering the lake water cavity. Specific conductivity and temperature
574 profiles from a CTD cast into the lake after drilling, but prior to water sampling, showed no
575 evidence for drill water incursion into the 15 m deep lake (99). Second, much of the water in the
576 borehole originates from melting of the ice sheet side wall, not hot water injected into the
577 borehole from the drill. Procedural blanks taken from a an access port on the hot water drilling

578 system of the borehole return water (Port 9, (18)) were very low compared to measured values
579 from the lake water (Table S3), with the exception of Zn, where blanks were ~40 nM (i.e. 55 %
580 of the dZn value at SLM). Finally, the Niskin bottle was slowly lowered to mid-depth in the lake
581 water column (lake water column = 15 m deep), hence, the bottle passed through ~7.5 m of lake
582 water flushing it more than 8 volumes of lake water before samples were collected.
583
584 **4.2.2 TE analytical procedures**
585 SLM samples were measured on a Thermo Scientific^{TM} Element 2^{TM} HR-ICP-MS (high
586 resolution inductively coupled mass spectrometer), and LG samples were measured on a Thermo
587 Scientific^{TM} XSERIES 2 quadrupole ICP-MS with collision/reaction cell. Be, In and Re were
588 used as internal standards to correct for drift and matrix effects (only In was used for SLM
589 samples), and eight multi-element external calibration solutions were made gravimetrically to
590 match the concentration range observed in samples. Measurement accuracy and precision were
591 checked against reference material NIST1643 (SLM), SLRS-5 (LG) or SLRS-6 (SLM; National
592 Research Council of Canada) and replicate intermediate standards. Analytical precision ranged
593 from ±0.7 % to ±8.9 % based on replicates of the SLRS-5 and a gravimetrically weighed
594 intermediate standard (n = 6 per run; Table S4), and ± 0.5 to ± 7.9 % based on replicates of
595 SLRS-6 (n = 5 per run; Table S5). There were two outliers to this; with Cd and Zn difficult to
596 quantify in LG samples, where precision was > ± 25 % due to the low concentrations and counts
597 per second (at or close to the instrumental detection limit). Accuracy was better than ± 10 % for
598 all elements apart from Cd (LG and SLM) and Zn (LG) as detailed in Table S4 and S5.
599
600 **4.2.3 Aqueous geochemical sampling, processing and analysis**

601 The determination of pH, specific conductivity (SC), oxygen, major ion chemistry, dissolved
602 organic carbon (DOC) concentration and suspended sediment concentration (SSC) for samples
603 from LG has been previously described (42, 49, 56). Aqueous geochemical parameters were
604 measured on samples from SLM as follows; pH, casts 2, 3, SPC and major ion chemistry, casts
605 1-6, DOC, dissolved inorganic carbon (DIC) and alkalinity, casts 1-3, 5, 6, SSC, cast 1. pH was
606 measured using an Accumet™ pH electrode, connected to an Accumet™ AB15 pH meter with
607 internal temperature compensation, standardized with Orion™ Pure Water™ pH buffers
608 immediately prior to sample measurement. Additional verification of pH was conducted with the
609 CO2sys software (Excel version 1.02) using measured DIC and alkalinity and the freshwater
610 option (salinity = 0) for dissociation constants of carbonic acid (100). Specific conductivity (at
611 25 ^{o}C) was measured using a YSI 3200 conductivity probe connected to a YSI Model 3100
612 conductivity meter calibrated immediately prior to sample measurement. Samples for major ion
613 chemistry were vacuum filtered through 0.4 µm Nuclepore™ membranes into clean 60 ml HDPE
614 bottles, pre-rinsed with filtered sample and stored frozen until analysis. Major ion concentrations
615 were determined on a Metrohm 930 Compact IC Flex ion chromatograph using Metrosep C4
616 cation and A SUPP 5 anion columns (38). Suspended sediment concentration was determined
617 gravimetrically using a pre-weighed Nuclepore™ membrane, after drying at 40^{o}C for 16 hours.
618 Alkalinity was measured by acid neutralization to pH 4.5, using bromocresol green-methyl red
619 indicator powder pillows (Permachem® reagent 94399) to detect the endpoint. A micro-pipette
620 was used to dispense µl volumes of 0.16 N H_2SO_4 into a ~25 ml lake water sample. Volumes of
621 acid and lakewater were determined gravimetrically. DIC was measured by infrared gas analysis
622 of acid sparged sub-samples from aliquots collected in gas tight serum vials. Samples for
623 determination of DOC concentrations were filtered, stored and analyzed as described in (15).

624 Oxygen concentrations were measured using a modified Winkler titration (Limnological
625 Methods for the McMurdo Long Term Ecological Research Program; (101)).
626
627 **Acknowledgements**
628 This research is part of a European Commission Horizon 2020 Marie Skłodowska-Curie Actions
629 fellowship ICICLES (grant agreement #793962) to JRH. Antarctic work was funded under the
630 Subglacial Antarctic Lakes Scientific Access (SALSA) project through U.S. NSF grants
631 1543537 to JCP, JED and MLS, and 1543453 to WBL. AS was supported by a NASA NESSF
632 fellowship (80NSSC18K1266). The Greenland research was funded by a U.K. NERC Standard
633 Grant (NE/I008845/1) to JLW and MT, a Leverhulme Trust Research Grant (RPG-2016-439) to
634 JLW, and a Royal Society Wolfson Merit Award to JLW. The authors thank all those involved
635 with fieldwork at Leverett camp and the SALSA project. We also thank A. Chiuchiolo for
636 conducting dissolved inorganic carbon analysis for SALSA, and analytical support from Dr. M.
637 Cooper at the National Oceanography Centre, U.K., Plasma Mass Spectrometry Lab, and G.
638 White in the geochemistry group at the National High Magnetic Field Geochemistry Laboratory,
639 which is supported by NSF DMR-1644779 and the State of Florida. We are extremely grateful
640 for the comments and input from T. Vick-Majors, R. Venturelli and G. Lamarche-Gagnon on an
641 earlier draft of the manuscript. The SALSA Science Team consists of T. Campbell, B. Christner,
642 C. Davis, H. Fricker, D. Harwood, A. Leventer, W. Li, A. Michaud, M. Patterson, B. Rosenheim,
643 M. Siegfried, R. Venturelli and T. Vick-Majors.
644
645 **Author contributions**

JRH, MLS, JLW and JCP conceived the project. JRH, MLS, JCP, JEH, CBG, TJK, MS, EAB, JB, JED and MT performed the fieldwork, collected samples and undertook field measurements. JRH, PLM, AS, JED, JB and MT undertook the geochemical analyses. JCP, MLS, JED, JLW, MT, WBL, RGMS and JRH funded the research. JRH analyzed the data and wrote the manuscript with significant input from MLS, JLW, JCP, MT and RGMS, and contributions from all other co-authors.

Competing statement

The authors declare no competing interests.

REFERENCES CITED

1. J. L. Wadham *et al.*, Ice sheets matter for the global carbon cycle. *Nat. Commun.* **10**, 3567-3567 (2019).
2. J. L. Bamber, R. M. Westaway, B. Marzeion, B. Wouters, The land ice contribution to sea level during the satellite era. *Environ Res Lett* **13**, 063008 (2018).
3. B. Smith *et al.*, Pervasive ice sheet mass loss reflects competing ocean and atmosphere processes. *Science* 10.1126/science.aaz5845, eaaz5845 (2020).
4. D. W. Ashmore, R. G. Bingham, Antarctic subglacial hydrology: current knowledge and future challenges. *Antarct Sci* **26**, 758-773 (2014).
5. M. J. Siegert, N. Ross, A. M. Le Brocq, Recent advances in understanding Antarctic subglacial lakes and hydrology. *Philosophical Transactions of the Royal Society of London A: Mathematical, Physical and Engineering Sciences* **374** (2016).
6. J. S. Bowling, S. J. Livingstone, A. J. Sole, W. Chu, Distribution and dynamics of Greenland subglacial lakes. *Nat. Commun.* **10**, 2810 (2019).
7. S. P. Carter, H. A. Fricker, The supply of subglacial meltwater to the grounding line of the Siple Coast, West Antarctica. *Ann Glaciol* **53**, 267-280 (2012).
8. J. C. Priscu *et al.*, "Antarctic subglacial water: origin, evolution, and ecology" in Polar Lakes and Rivers, W. F. Vincent, J. Laybourn-Parry, Eds. (Oxford University Press, Oxford, 2008), vol. 1, pp. 119-137.
9. A. Urra *et al.*, Weathering Dynamics Under Contrasting Greenland Ice Sheet Catchments. *Frontiers in Earth Science* **7** (2019).
10. M. Sharp, M. Tranter, Glacier biogeochemistry. *Geochem. Perspect.* 10.7185/geochempersp.6.2 (2017).
11. T. Cowton, P. Nienow, I. Bartholomew, A. Sole, D. Mair, Rapid erosion beneath the Greenland ice sheet. *Geology* **40**, 343-346 (2012).
12. M. Tranter, J. L. Wadham, "Geochemical Weathering in Glacial and Proglacial Environments" in Treatise on Geochemistry (Second Edition), H. D. Turekian, K. K. Holland, Eds. (Elsevier, Oxford, 2014), http://dx.doi.org/10.1016/B978-0-08-095975-7.00505-2, pp. 157-173.
13. J. R. Hawkings *et al.*, The effect of warming climate on nutrient and solute export from the Greenland Ice Sheet. *Geochem. Perspect. Lett.* **1**, 94-104 (2015).
14. E. Hood, T. J. Battin, J. Fellman, S. O'Neel, R. G. M. Spencer, Storage and release of organic carbon from glaciers and ice sheets. *Nat. Geosci.* **8**, 91-96 (2015).
15. T. J. Vick-Majors *et al.*, Biogeochemical Connectivity Between Freshwater Ecosystems beneath the West Antarctic Ice Sheet and the Sub-Ice Marine Environment. *Global Biogeochem. Cy.* **34**, e2019GB006446 (2020).
16. J. C. Yde, N. T. Knudsen, B. Hasholt, A. B. Mikkelsen, Meltwater chemistry and solute export from a Greenland Ice Sheet catchment, Watson River, West Greenland. *J Hydrol* **519, Part B**, 2165-2179 (2014).
17. J. C. Priscu *et al.*, A microbiologically clean strategy for access to the Whillans Ice Stream subglacial environment. *Antarct Sci* **25**, 637-647 (2013).
18. A. B. Michaud *et al.*, Environmentally clean access to Antarctic subglacial aquatic environments. *Antarct Sci* 10.1017/S0954102020000231, 1-12 (2020).

19. M. J. Hopwood *et al.*, Review article: How does glacier discharge affect marine biogeochemistry and primary production in the Arctic? *Cryosphere* **14**, 1347-1383 (2020).
20. A. C. Mitchell, G. H. Brown, Diurnal hydrological – physicochemical controls and sampling methods for minor and trace elements in an Alpine glacial hydrological system. *J Hydrol* **332**, 123-143 (2007).
21. S. M. Aciego, E. I. Stevenson, C. A. Arendt, Climate versus geological controls on glacial meltwater micronutrient production in southern Greenland. *Earth. Planet. Sc. Lett.* **424**, 51-58 (2015).
22. J. Gaillardet, J. Viers, B. Dupre, "Trace Elements in River Waters" in Treatise on Geochemistry, J. I. Drever, Ed. (Elsevier, 2014), vol. 5.
23. J. R. Hawkings *et al.*, Ice sheets as a significant source of highly reactive nanoparticulate iron to the oceans. *Nat. Commun.* **5** (2014).
24. C. B. Gardner *et al.*, Molybdenum, vanadium, and uranium weathering in small mountainous rivers and rivers draining high-standing islands. *Geochim. Cosmochim. Acta* **219**, 22-43 (2017).
25. A. M. Shiller, L. Mao, Dissolved vanadium in rivers: effects of silicate weathering. *Chem. Geol.* **165**, 13-22 (2000).
26. C. A. Miller, B. Peucker-Ehrenbrink, B. D. Walker, F. Marcantonio, Re-assessing the surface cycling of molybdenum and rhenium. *Geochim. Cosmochim. Acta* **75**, 7146-7179 (2011).
27. J. T. Cullen, M. T. Maldonado, "Biogeochemistry of Cadmium and Its Release to the Environment" in Cadmium: From Toxicity to Essentiality, A. Sigel, H. Sigel, R. K. O. Sigel, Eds. (Springer Netherlands, Dordrecht, 2013), 10.1007/978-94-007-5179-8_2, pp. 31-62.
28. A. M. Shiller, Dissolved trace elements in the Mississippi River: Seasonal, interannual, and decadal variability. *Geochim. Cosmochim. Acta* **61**, 4321-4330 (1997).
29. M. M. Benjamin, J. O. Leckie, Multiple-site adsorption of Cd, Cu, Zn, and Pb on amorphous iron oxyhydroxide. *J Colloid Interf Sci* **79**, 209-221 (1981).
30. M. R. Palmer, J. M. Edmond, Uranium in river water. *Geochim. Cosmochim. Acta* **57**, 4947-4955 (1993).
31. M. R. Palmer, J. M. Edmond, The strontium isotope budget of the modern ocean. *Earth. Planet. Sc. Lett.* **92**, 11-26 (1989).
32. F. M. M. Morel, A. J. Milligan, M. A. Saito, "8.5 - Marine Bioinorganic Chemistry: The Role of Trace Metals in the Oceanic Cycles of Major Nutrients" in Treatise on Geochemistry (Second Edition), H. D. Holland, K. K. Turekian, Eds. (Elsevier, Oxford, 2014), https://doi.org/10.1016/B978-0-08-095975-7.00605-7, pp. 123-150.
33. M. C. Lohan, A. Tagliabue, Oceanic Micronutrients: Trace Metals that are Essential for Marine Life. *Elements* **14**, 385-390 (2018).
34. B. S. Twining, S. B. Baines, The Trace Metal Composition of Marine Phytoplankton. *Annu Rev Mar Sci* **5**, 191-215 (2013).
35. C. M. Moore *et al.*, Processes and patterns of oceanic nutrient limitation. *Nat. Geosci.* **6**, 701-710 (2013).
36. T. M. Downs, M. Schallenberg, C. W. Burns, Responses of lake phytoplankton to micronutrient enrichment: a study in two New Zealand lakes and an analysis of published data. *Aquat Sci* **70**, 347-360 (2008).

37. J. A. Graly, N. F. Humphrey, C. M. Landowski, J. T. Harper, Chemical weathering under the Greenland Ice Sheet. *Geology* **42**, 551-554 (2014).
38. A. B. Michaud *et al.*, Solute sources and geochemical processes in Subglacial Lake Whillans, West Antarctica. *Geology* **44**, 347-350 (2016).
39. J. R. Hawkings *et al.*, Biolabile ferrous iron bearing nanoparticles in glacial sediments. *Earth. Planet. Sc. Lett.* **493**, 92-101 (2018).
40. R. Raiswell *et al.*, Iron in Glacial Systems: Speciation, Reactivity, Freezing Behavior, and Alteration During Transport. *Frontiers in Earth Science* **6** (2018).
41. M. R. Siegfried, H. A. Fricker, Thirteen years of subglacial lake activity in Antarctica from multi-mission satellite altimetry. *Ann Glaciol* **59**, 42-55 (2018).
42. J. E. Hatton *et al.*, Investigation of subglacial weathering under the Greenland Ice Sheet using silicon isotopes. *Geochim. Cosmochim. Acta* **247**, 191-206 (2019).
43. J. R. Hawkings *et al.*, Ice sheets as a missing source of silica to the polar oceans. *Nat. Commun.* **8**, 14198 (2017).
44. H. H. Durr, M. Meybeck, J. Hartmann, G. G. Laruelle, V. Roubeix, Global spatial distribution of natural riverine silica inputs to the coastal zone. *Biogeosciences* **8**, 597-620 (2011).
45. R. L. Rudnick, S. Gao, "Composition of the Continental Crust" in Treatise on Geochemistry (Second Edition), H. D. Holland, K. K. Turekian, Eds. (Elsevier, Oxford, 2014), http://dx.doi.org/10.1016/B978-0-08-095975-7.00301-6, pp. 1-51.
46. J. L. Wadham *et al.*, Biogeochemical weathering under ice: Size matters. *Global Biogeochem. Cy.* **24**, GB3025 (2010).
47. R. S. Hindshaw, J. Rickli, J. Leuthold, J. Wadham, B. Bourdon, Identifying weathering sources and processes in an outlet glacier of the Greenland Ice Sheet using Ca and Sr isotope ratios. *Geochim. Cosmochim. Acta* **145**, 50-71 (2014).
48. E. I. Stevenson, M. S. Fantle, S. B. Das, H. M. Williams, S. M. Aciego, The iron isotopic composition of subglacial streams draining the Greenland ice sheet. *Geochim. Cosmochim. Acta* **213**, 237-254 (2017).
49. A. M. Kellerman *et al.*, Glacier Outflow Dissolved Organic Matter as a Window Into Seasonally Changing Carbon Sources: Leverett Glacier, Greenland. *Journal of Geophysical Research: Biogeosciences* **125**, e2019JG005161 (2020).
50. V. Barrón, J. Torrent (2013) Iron, manganese and aluminium oxides and oxyhydroxides. in *Minerals at the Nanoscale*, eds F. Nieto, K. J. T. Livi, R. Oberti (Mineralogical Society of Great Britain and Ireland), p 0.
51. G. Olivié-Lauquet, T. Allard, J. Bertaux, J.-P. Muller, Crystal chemistry of suspended matter in a tropical hydrosystem, Nyong basin (Cameroon, Africa). *Chem. Geol.* **170**, 113-131 (2000).
52. J. P. Stegemeier, B. C. Reinsch, C. J. Lentini, J. G. Dale, C. S. Kim, Aggregation of nanoscale iron oxyhydroxides and corresponding effects on metal uptake, retention, and speciation: II. Temperature and time. *Geochim. Cosmochim. Acta* **148**, 113-129 (2015).
53. J. G. Dale, J. P. Stegemeier, C. S. Kim, Aggregation of nanoscale iron oxyhydroxides and corresponding effects on metal uptake, retention, and speciation: I. Ionic-strength and pH. *Geochim. Cosmochim. Acta* **148**, 100-112 (2015).
54. M. F. Hochella *et al.*, Nanominerals, Mineral Nanoparticles, and Earth Systems. *Science* **319**, 1631 (2008).

55. H. Pryer *et al.*, Glacial Cover Affects Silicon and Iron Exports from Rivers in Chilean Patagonia. *Global Biogeochem. Cy.* (in review).
56. A. D. Beaton *et al.*, High-Resolution in Situ Measurement of Nitrate in Runoff from the Greenland Ice Sheet. *Environ Sci Technol* **51**, 12518-12527 (2017).
57. J. Wadham *et al.*, The potential role of the Antarctic Ice Sheet in global biogeochemical cycles. *Earth Env Sci T R So* **104**, 55-67 (2013).
58. K.-U. Ulrich, A. Rossberg, H. Foerstendorf, H. Zänker, A. C. Scheinost, Molecular characterization of uranium(VI) sorption complexes on iron(III)-rich acid mine water colloids. *Geochim. Cosmochim. Acta* **70**, 5469-5487 (2006).
59. S. J. Markich, Uranium Speciation and Bioavailability in Aquatic Systems: An Overview. *TheScientificWorldJOURNAL* **2**, 756147 (2002).
60. K. Saeki, S.-I. Wada, M. Shibata, Ca2+-Fe2+ and Ca2+-Mn2+ exchange selectivitiy of kaolinite, montmorillonite, and illite. *Soil Sci* **169**, 125-132 (2004).
61. D. M. Chandler *et al.*, Evolution of the subglacial drainage system beneath the Greenland Ice Sheet revealed by tracers. *Nat. Geosci.* **6**, 195-198 (2013).
62. G. Lamarche-Gagnon *et al.*, Greenland melt drives continuous export of methane from the ice-sheet bed. *Nature* **565**, 73-77 (2019).
63. J. F. Pankow, J. J. Morgan, Kinetics for the aquatic environment - manganese. *Environ Sci Technol* **15**, 1306-1313 (1981).
64. R. D. Cody, Adsorption and the reliability of trace elements as environment indicators for shales. *J Sediment Res* **41**, 461-471 (1971).
65. T. J. Kohler *et al.*, Carbon dating reveals a seasonal progression in the source of particulate organic carbon exported from the Greenland Ice Sheet. *Geophys. Res. Lett.* **44**, 6209-6217 (2017).
66. A. Tagliabue *et al.*, The Role of External Inputs and Internal Cycling in Shaping the Global Ocean Cobalt Distribution: Insights From the First Cobalt Biogeochemical Model. *Global Biogeochem. Cy.* **32**, 594-616 (2018).
67. M. P. Bhatia *et al.*, Greenland meltwater as a significant and potentially bioavailable source of iron to the ocean. *Nat. Geosci.* **6**, 274-278 (2013).
68. P. J. Statham, M. Skidmore, M. Tranter, Inputs of glacially derived dissolved and colloidal iron to the coastal ocean and implications for primary productivity. *Global Biogeochem. Cy.* **22**, GB3013 (2008).
69. A. Hodson *et al.*, Climatically sensitive transfer of iron to maritime Antarctic ecosystems by surface runoff. *Nat. Commun.* **8**, 14499 (2017).
70. P. van der Merwe *et al.*, High Lability Fe Particles Sourced From Glacial Erosion Can Meet Previously Unaccounted Biological Demand: Heard Island, Southern Ocean. *Frontiers in Marine Science* **6**, 332-332 (2019).
71. M. J. Hopwood *et al.*, Highly variable iron content modulates iceberg-ocean fertilisation and potential carbon export. *Nat. Commun.* **10**, 5261 (2019).
72. R. Raiswell *et al.*, Potentially bioavailable iron delivery by iceberg-hosted sediments and atmospheric dust to the polar oceans. *Biogeosciences* **13**, 3887-3900 (2016).
73. A. Dai, K. E. Trenberth, Estimates of freshwater discharge from continents: Latitudinal and seasonal variations. *J Hydrometeorol* **3**, 660-687 (2002).
74. M. J. Hopwood *et al.*, Seasonal Changes in Fe along a Glaciated Greenlandic Fjord. *Frontiers in Earth Science* **4** (2016).

75. A. W. Schroth, J. Crusius, I. Hoyer, R. Campbell, Estuarine removal of glacial iron and implications for iron fluxes to the ocean. *Geophys. Res. Lett.* **41**, 3951-3958 (2014).
76. J. L. Wadham *et al.*, Sources, cycling and export of nitrogen on the Greenland Ice Sheet. *Biogeosciences* **13**, 6339-6352 (2016).
77. J. Hawkings *et al.*, The Greenland Ice Sheet as a hotspot of phosphorus weathering and export in the Arctic. *Global Biogeochem. Cy.* **30**, 191-210 (2016).
78. K. W. Bruland, R. Middag, M. C. Lohan, "Controls of Trace Metals in Seawater" in Treatise on Geochemistry (Second Edition), H. D. Holland, K. K. Turekian, Eds. (Elsevier, Oxford, 2014), https://doi.org/10.1016/B978-0-08-095975-7.00602-1, pp. 19-51.
79. K. W. Bruland *et al.*, Factors influencing the chemistry of the near-field Columbia River plume: Nitrate, silicic acid, dissolved Fe, and dissolved Mn. *Journal of Geophysical Research: Oceans* **113** (2008).
80. L. Meire *et al.*, Marine-terminating glaciers sustain high productivity in Greenland fjords. *Global Change Biol.* **23**, 5344-5357 (2017).
81. K. R. Arrigo, G. L. van Dijken, A. L. Strong, Environmental controls of marine productivity hot spots around Antarctica. *Journal of Geophysical Research: Oceans* 10.1002/2015JC010888, n/a-n/a (2015).
82. M. van Hulten *et al.*, Manganese in the west Atlantic Ocean in the context of the first global ocean circulation model of manganese. *Biogeosciences* **14**, 1123-1152 (2017).
83. C. Richon, A. Tagliabue, Insights Into the Major Processes Driving the Global Distribution of Copper in the Ocean From a Global Model. *Global Biogeochem. Cy.* **33**, 1594-1610 (2019).
84. J. H. Martin, S. E. Fitzwater, R. M. Gordon, Iron deficiency limits phytoplankton growth in Antarctic waters. *Global Biogeochem. Cy.* **4**, 5-12 (1990).
85. A. L. Annett *et al.*, Controls on dissolved and particulate iron distributions in surface waters of the Western Antarctic Peninsula shelf. *Mar. Chem.* https://doi.org/10.1016/j.marchem.2017.06.004 (2017).
86. L. J. A. Gerringa *et al.*, Iron from melting glaciers fuels the phytoplankton blooms in Amundsen Sea (Southern Ocean): Iron biogeochemistry. *Deep Sea Res Part II Top Stud Oceanogr.* **71-76**, 16-31 (2012).
87. R. Death *et al.*, Antarctic ice sheet fertilises the Southern Ocean. *Biogeosciences* **11**, 2635-2643 (2014).
88. R. Person *et al.*, Sensitivity of ocean biogeochemistry to the iron supply from the Antarctic Ice Sheet explored with a biogeochemical model. *Biogeosciences* **16**, 3583-3603 (2019).
89. A. M. Shiller, Syringe Filtration Methods for Examining Dissolved and Colloidal Trace Element Distributions in Remote Field Locations. *Environ Sci Technol* **37**, 3953-3957 (2003).
90. C. Laufkötter, A. A. Stern, J. G. John, C. A. Stock, J. P. Dunne, Glacial Iron Sources Stimulate the Southern Ocean Carbon Cycle. *Geophys. Res. Lett.* **45**, 13,377-313,385 (2018).
91. L. Herraiz-Borreguero, D. Lannuzel, P. van der Merwe, A. Treverrow, J. B. Pedro, Large flux of iron from the Amery Ice Shelf marine ice to Prydz Bay, East Antarctica. *Journal of Geophysical Research: Oceans* **121**, 6009-6020 (2016).

881 92. G. A. Cutter, Trace Elements in Estuarine and Coastal Waters - U.S. Studies from 1986–
882 1990. *Reviews of Geophysics* **29**, 639-644 (1991).
883 93. M. R. Cape, F. Straneo, N. Beaird, R. M. Bundy, M. A. Charette, Nutrient release to
884 oceans from buoyancy-driven upwelling at Greenland tidewater glaciers. *Nat. Geosci.* **12**,
885 34-39 (2019).
886 94. K. Kunde *et al.*, Iron Distribution in the Subtropical North Atlantic: The Pivotal Role of
887 Colloidal Iron. *Global Biogeochem. Cy.* **33**, 1532-1547 (2019).
888 95. S. P. Carter, H. A. Fricker, M. R. Siegfried, Evidence of rapid subglacial water piracy
889 under Whillans Ice Stream, West Antarctica. *J. Glaciol.* **59**, 1147-1162 (2013).
890 96. M. R. Siegfried *et al.* (2019) Anatomy of a draining subglacial lake in West Antarctica. in
891 *AGU Fall Meeting* (San Francisco, CA).
892 97. S. Anandakrishnan, D. D. Blankenship, R. B. Alley, P. L. Stoffa, Influence of subglacial
893 geology on the position of a West Antarctic ice stream from seismic observations. *Nature*
894 **394**, 62-65 (1998).
895 98. N. Henriksen, A. K. Higgins, F. Kalsbeek, T. C. R. Pulvertaft, Greenland from Archaean
896 to Quaternary Descriptive text to the 1995 Geological map of Greenland, 1:2 500 000.
897 2nd edition. *Geol Surv Den Greenl*, 9-116 (2009).
898 99. J. Priscu *et al.*, Scientific Access into Mercer Subglacial Lake: Scientific Objectives,
899 Drilling Operations and Initial Observations. *Ann Glaciol* (in review).
900 100. D. Pierrot, E. Lewis, D. W. R. Wallace (2006) MS Excel program developed for CO2
901 system calculations. (ORNL/CDIAC-105, Carbon Dioxide Information Analysis Center,
902 Oak Ridge National Laboratory, U.S. Department of Energy, Oak Ridge, TN.).
903 101. J. H. Carpenter, THE CHESAPEAKE BAY INSTITUTE TECHNIQUE FOR THE
904 WINKLER DISSOLVED OXYGEN METHOD. *Limnol. Oceanogr.* **10**, 141-143 (1965).
905 102. F. Pattyn, Antarctic subglacial conditions inferred from a hybrid ice sheet/ice stream
906 model. *Earth. Planet. Sc. Lett.* **295**, 451-461 (2010).
907 103. A. Le Brocq *et al.*, Evidence from ice shelves for channelized meltwater flow beneath the
908 Antarctic Ice Sheet. *Nat. Geosci.* **6**, 945-948 (2013).
909 104. J. M. Martin, M. Meybeck, Elemental Mass-Balance of Material Carried by Major World
910 Rivers. *Mar. Chem.* **7**, 173-206 (1979).
911

Table 1: Estimates of annual fluxes of size fractionated TEs from the Greenland Ice Sheet and the Antarctic Ice Sheet. Elemental fluxes are present either as Mmol (10^6 mol) or Gmol (10^9 mol) per year. The mean is given in bold and estimated range/uncertainty are given in parentheses. Flux estimates are presented to 2 significant figures/decimal places.

Element/ variable	Unit	Greenland Ice Sheet [a]			Antarctic Ice Sheet [b]		
		d	cn	s	d	cn	s
Water flux	$km^3\ yr^{-1}$	560 (410 – 730) [c]			65 (32.5 – 97.5) [d]		
Al	$10^9\ mol\ yr^{-1}$	**9.2** (0.14 – 77)	**8.0** (0 – 74)	**1.31** (0 – 5.8)	**4.5** (2.1 – 7.1)	**4.2** (2.1 – 6.3)	**0.33** (0.15 – 0.53)
Ba	$10^6\ mol\ yr^{-1}$	**13** (1.3 – 60)	**11** (0.03 - 58.4)	**1.4** (0.23 – 22)	**7.6** (3.6 – 12)	**6.7** (3.3 – 10)	**0.91** (0.33 – 1.8)
Cd	$10^6\ mol\ yr^{-1}$	**0.01** (0 – 0.05)	**0** (0 – 0.02)	**0.01** (0 – 0.04)	**0.02** (0.01 – 0.02)	**0.01** (0 – 0.01)	**0** (0 – 0.01)
Co	$10^6\ mol\ yr^{-1}$	**0.86** (0.05 – 2.9)	**0.79** (0 – 2.8)	**0.07** (0.01 – 2.2)	**0.48** (0.24 – 0.73)	**0.48** (0.24 – 0.72)	**0** (0 – 0)
Cr	$10^6\ mol\ yr^{-1}$	**3.4** (0.08 – 17)	**3.2** (0.01 – 17)	**0.13** (0.01 – 1.6)	**2.2** (1.1 – 3.4)	**1.5** (0.78 – 2.3)	**0.68** (0.34 – 1.0)
Cu	$10^6\ mol\ yr^{-1}$	**5.9** (1.3 – 31)	**4.7** (0.56 – 17)	**1.2** (0.57 – 17)	**2.9** (1.4 – 4.3)	**2.6** (1.3 – 3.9)	**0.27** (0.13 – 0.41)
Fe	$10^9\ mol\ yr^{-1}$	**1.3** (0.02 – 5.5)	**1.3** (0.02 – 5.5)	**0.01** (0 – 0.05)	**1.4** (0.66 – 2.1)	**1.4** (0.66 – 2.1)	**0**
Li	$10^9\ mol\ yr^{-1}$	**0.06** (0.03 – 0.23)	**0.01** (0 – 0.15)	**0.05** (0.03 – 0.12)	**0.12** (0.06 – 0.18)	**0.02** (0.01 – 0.03)	**0.10** (0.05 – 0.16)
Mn	$10^6\ mol\ yr^{-1}$	**41** (9.6 – 380)	**27** (0.15 – 220)	**14** (2.3 – 370)	**27** (13 – 41)	**27** (13 – 40)	**0.03** (0.01 – 0.04)
Mo	$10^6\ mol\ yr^{-1}$	**2.4** (0.78 – 8.3)	**0**	**2.4** (0.78 – 8.3)	**3.4** (1.7 – 5.2)	**0**	**3.4** (1.7 – 5.2)
Ni	$10^6\ mol\ yr^{-1}$	**7.0** (0.48 – 14)	**6.4** (0 – 13)	**0.61** (0.25 – 12)	**0.94** (0.47 – 1.4)	**0.86** (0.43 – 1.3)	**0.08** (0.04 – 0.12)
Pb	$10^6\ mol\ yr^{-1}$	**0.11** (0 – 0.49)	**0.10** (0 – 0.48)	**0.01** (0 – 0.02)	**0.32** (0.16 – 0.48)	**0.32** (0.16 – 0.48)	**0**
Sr	$10^9\ mol\ yr^{-1}$	**0.03** (0.02 – 0.14)	**0**	**0.03** (0.02 – 0.14)	**0.05** (0.03 – 0.08)	**0**	**0.05** (0.03 – 0.08)
Ti	$10^6\ mol\ yr^{-1}$	**160** (2.2 – 610)	**140** (1.1 – 600)	**1.2** (0.51 – 3.7)	**140** (65 – 210)	**140** (65 – 210)	**0**
U	$10^6\ mol\ yr^{-1}$	**0.07** (0.02 – 0.55)	**0.06** (0.02 – 0.48)	**0** (0 – 0.07)	**1.9** (0.95 – 2.9)	**0**	**1.9** (0.95 – 2.9)
V	$10^6\ mol\ yr^{-1}$	**17** (1.4 – 65)	**5.0** (0 – 48)	**12** (1.3 – 23)	**17** (8.6 – 26)	**4.2** (2.1 – 6.3)	**13** (6.5 – 20)
Zn	$10^6\ mol\ yr^{-1}$	**3.9** (0 – 20)	**3.9** (0 – 20)	**0.08** (0 – 1.5)	**4.7** (2.0 – 7.9)	**4.3** (2.1 – 7.2)	**0.38** (0.17 – 0.63)

[a] Elemental flux estimates from GrIS are derived from the minimum, discharge-weighted mean and maximum concentrations measured at LG multiplied by the modeled minimum, mean and maximum 2007-2016 ice sheet meltwater discharge.

[b] Elemental flux estimates from AIS are derived from the minimum, mean and maximum concentrations measured at SLM multiplied by the modeled minimum, mean and maximum AIS discharge.

[c] Mean modeled Greenland Ice Sheet meltwater discharge over 2007-2016 from (2). Min is the lowest melt year (2013), max is the largest melt year (2012).

[d] Modeling basal melt rates from (102) with a standard deviation of ± 50 %

Figure 1: Map of study regions. (a) Leverett Glacier, draining the Greenland Ice Sheet, and (b) Mercer Subglacial Lake, draining the Mercer Ice Stream. Water flows into the Watson River and then Søndre Strømfjord in (a). Modeled water flow paths into the Ross Ice Shelf cavity are indicated by the blue lines in (b) (103). SLW = Whillans Subglacial Lake, SLC = Conway Subglacial Lake, USLC = Upper Conway Subglacial Lake, SLE = Engelhardt Subglacial Lake, L8…12 = Lake 8…12. Insert polar stereographic maps are cut at (a) 60°N and (b) 60°S with study areas in shaded boxes. Topographic contours of the ice sheet surface (Greenland) or bed (Antarctic) are at 100 m intervals.

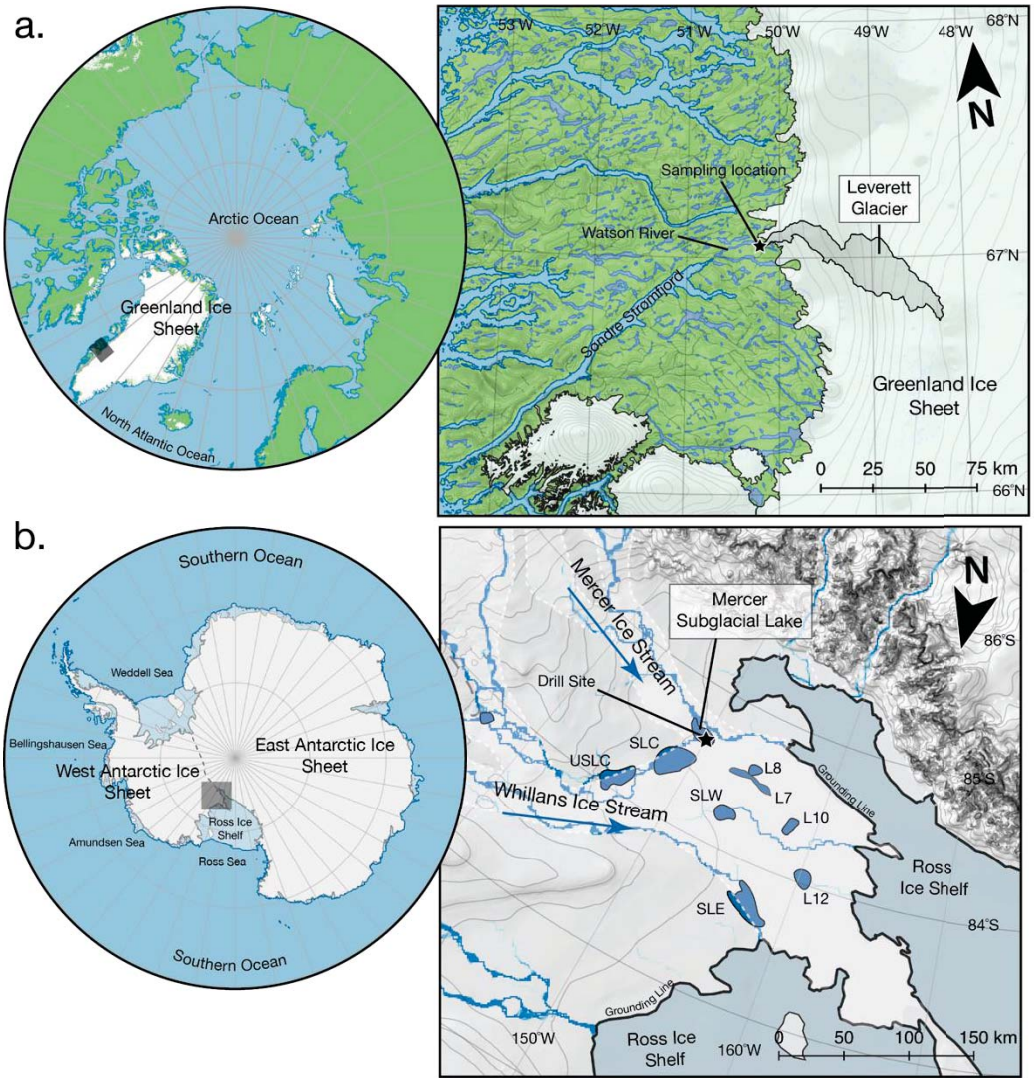

Figure 2: (a) Dissolved (<0.45 µm) mean elemental concentrations on a log scale in Leverett Glacier and Mercer Subglacial Lake samples, and either minimum/maximum range (Leverett Glacier) or standard deviations (Mercer Subglacial Lake), compared to best-estimate mean riverine concentrations (<0.2-0.45 µm)(22, 104). (b) Leverett Glacier and Mercer Subglacial Lake molar concentrations normalized to the global riverine mean dissolved elemental concentration (22, 104). Values of >1 equal enrichment compared to mean riverine waters. Values <1 indicate depletion compared to mean riverine waters. The grey region indicates values ±50 % of the riverine mean. (c) Mean Mercer Subglacial Lake concentrations normalized to Leverett Glacier concentrations. Leverett Glacier DOC and major ion/Si data from (42, 49). Elements are arranged along the X-axis from lowest mean non-glacial riverine concentration to highest non-glacial mean riverine concentration. n.b., Pb, Cd and Zn minimum concentrations at Leverett Glacier are below the limit of detection.

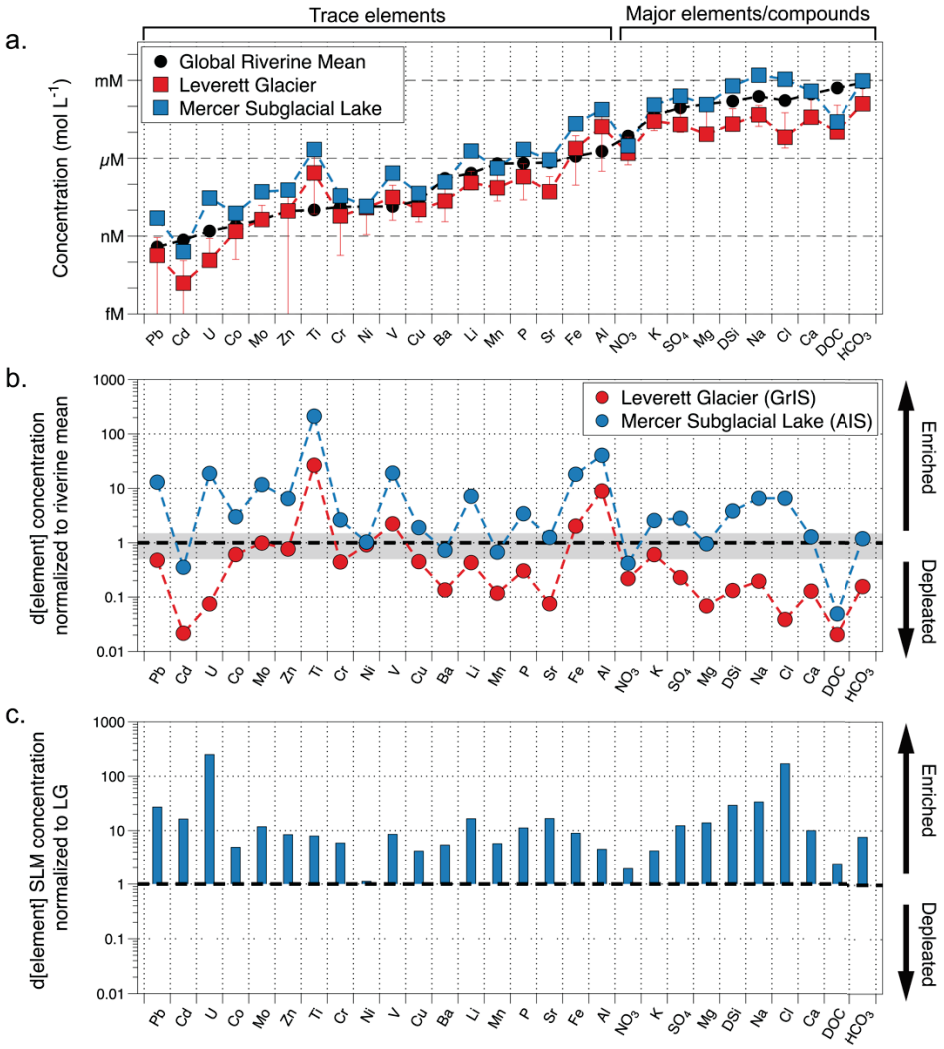

949 **Figure 3:** The proportion of colloidal/nanoparticulate (cn) and soluble (s) trace element species
950 in ice sheet meltwaters as a percentage of the <0.45 µm concentration. Ordering from left to right
951 on the x-axis is according to the percentage of the <0.45 µm fraction that is filterable through a
952 0.02 µm pore size (i.e., our best approximation of truly dissolved species) in Greenland Ice Sheet
953 samples with the highest on the left, and lowest on the right. Elemental groupings are indicated
954 on the right and with the horizontal dashed lines, and are detailed in the text.
955

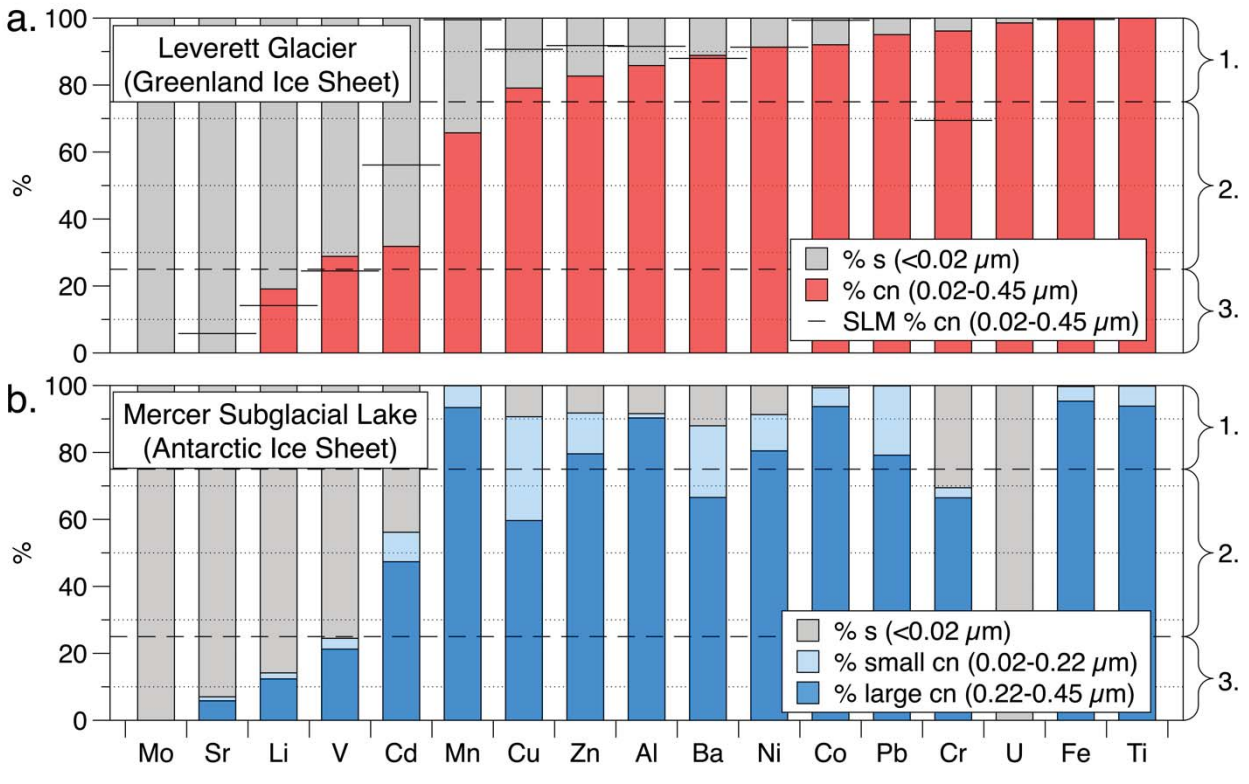

956
957
958

Figure 4: Mobility index of (a) highly mobile and (b) less mobile elements in the dissolved size fraction (<0.45 µm). Mobility index calculated via normalization of dissolved concentrations to upper continental crust abundance (22, 45, 104), with values normalized again to Na (thus Na = 1 in all environments). Higher values indicate greater elemental mobility from weathering. Elements are grouped and arranged according to mean riverine mobility (22) with least to most mobile elements in the <0.45 µm size fraction going from left to right on the X-axis.

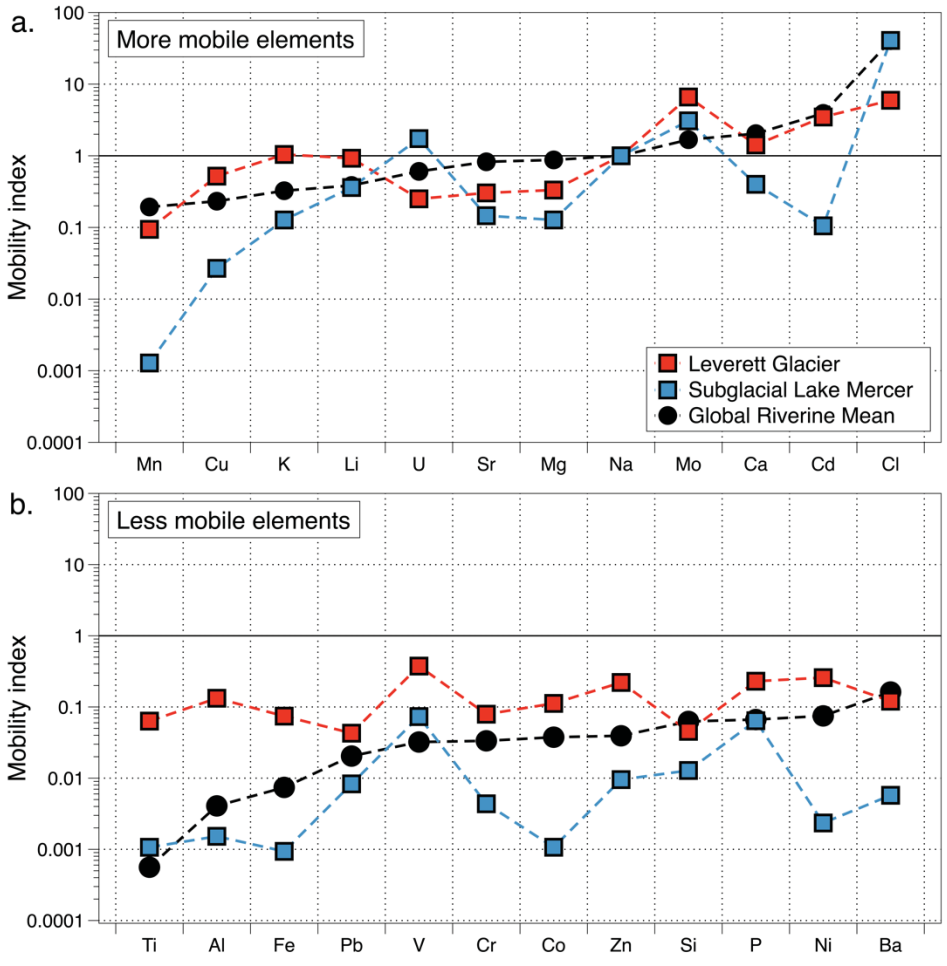

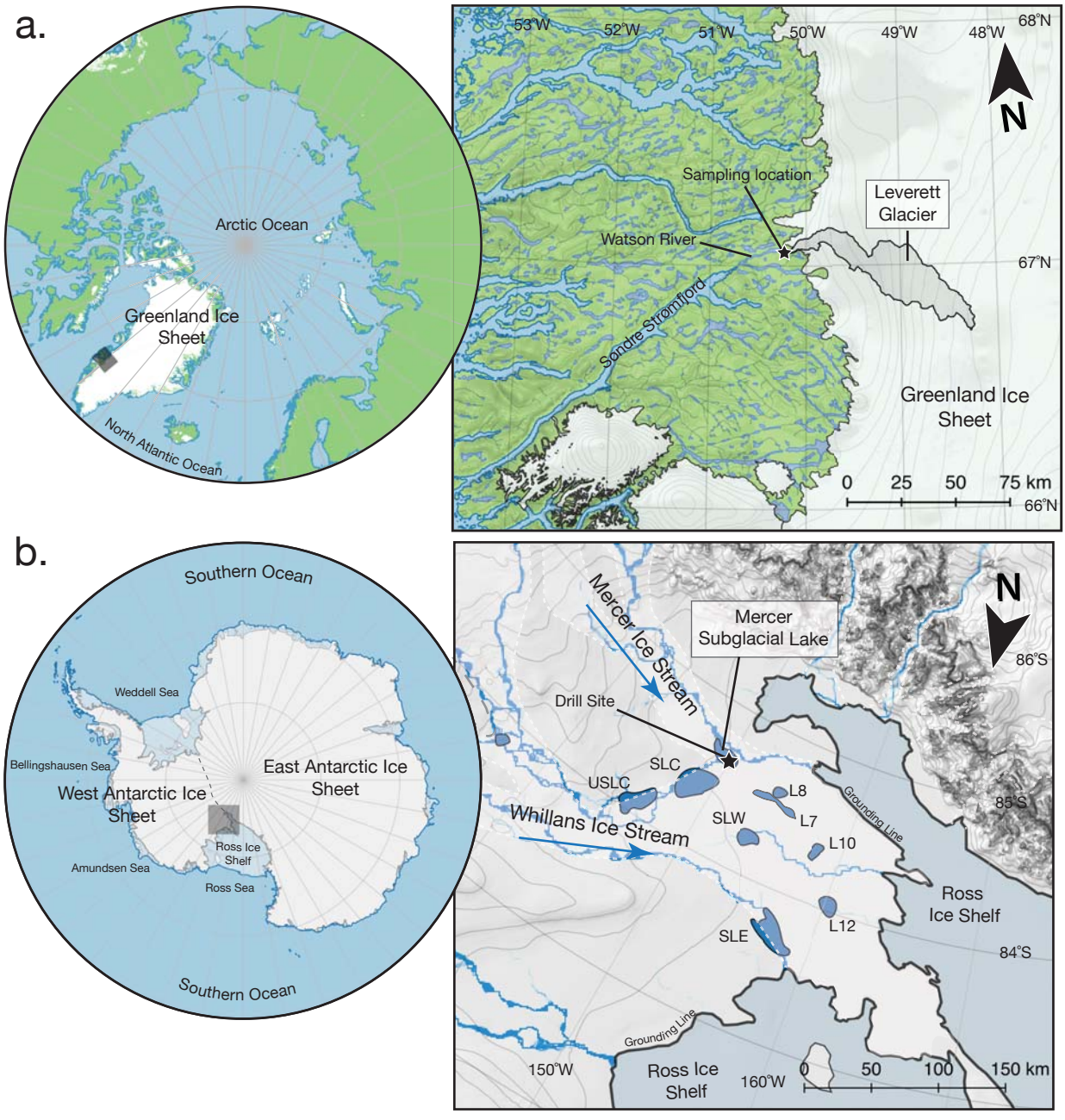
a.
Arctic Ocean
Greenland Ice Sheet
North Atlantic Ocean
53°W
52°W
51°W
50°W
49°W
48°W
68°N
N
Sampling location
Leverett Glacier
Watson River
67°N
Søndre Strømfjord
Greenland Ice Sheet
0 25 50 75 km
66°N
b.
Southern Ocean
Weddell Sea
Bellingshausen Sea
East Antarctic Ice Sheet
West Antarctic Ice Sheet
Ross Ice Shelf
Amundsen Sea
Ross Sea
Southern Ocean
Mercer Ice Stream
Mercer Subglacial Lake
N
86°S
Drill Site
SLC
USLC
L8
L7
SLW
Whillans Ice Stream
L10
Grounding Line
85°S
Ross Ice Shelf
L12
SLE
84°S
Grounding Line
150°W
Ross Ice Shelf
160°W
0 50 100 150 km

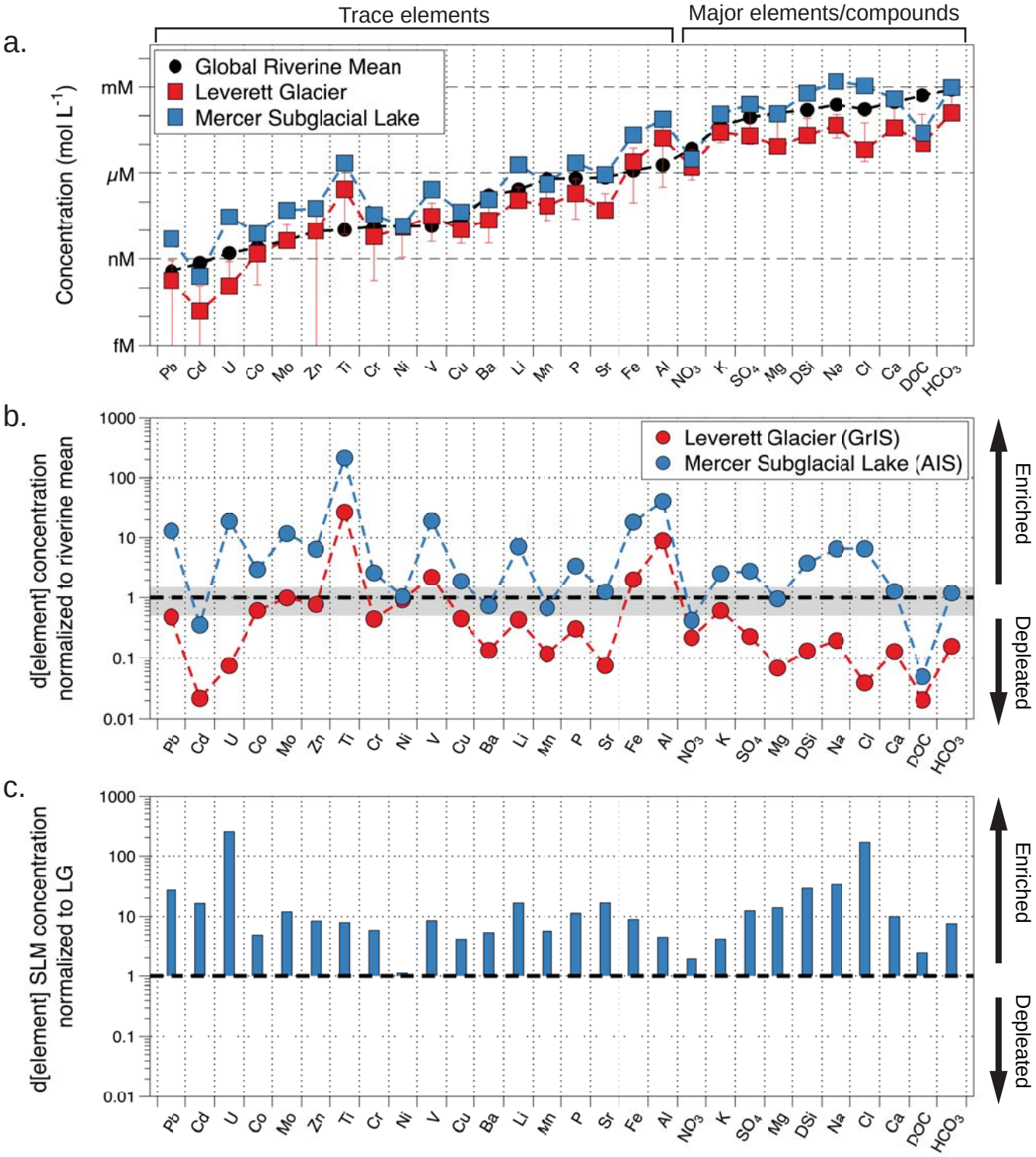
a.
Trace elements
Major elements/compounds
Global Riverine Mean
Leverett Glacier
Mercer Subglacial Lake
Concentration (mol L-1)
mM
μM
nM
fM
Pb Cd U Co Mo Zn Ti Cr Ni V Cu Ba Li Mn P Sr Fe Al NO3 K SO4 Mg DSi Na Cl Ca DOC HCO3
b.
d[element] concentration normalized to riverine mean
Leverett Glacier (GrIS)
Mercer Subglacial Lake (AIS)
Enriched
Depleated
1000
100
10
1
0.1
0.01
c.
d[element] SLM concentration normalized to LG
Enriched
Depleated

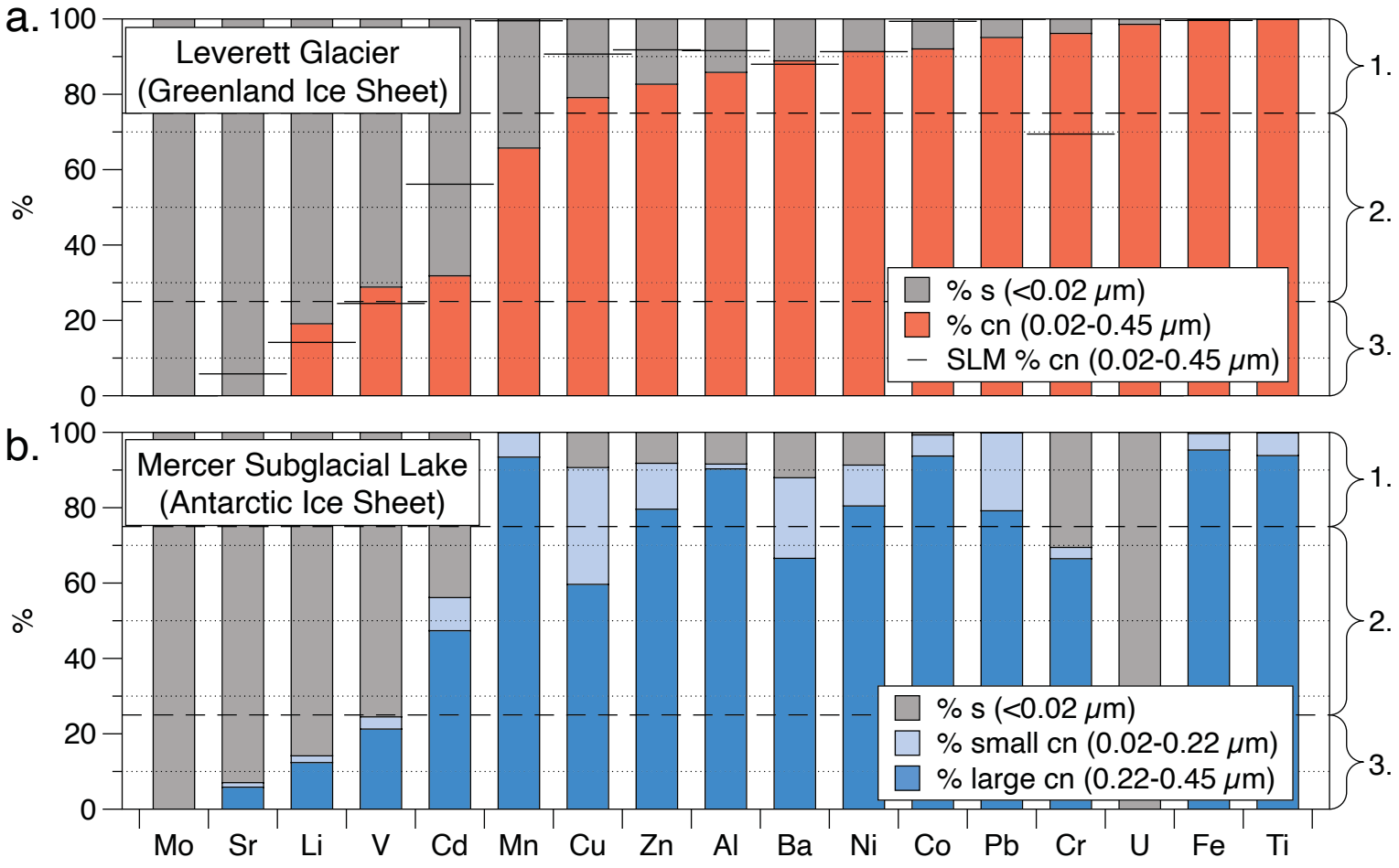
a.
Leverett Glacier
(Greenland Ice Sheet)
% s (<0.02 μm)
% cn (0.02-0.45 μm)
SLM % cn (0.02-0.45 μm)
b.
Mercer Subglacial Lake
(Antarctic Ice Sheet)
% s (<0.02 μm)
% small cn (0.02-0.22 μm)
% large cn (0.22-0.45 μm)
%
100
80
60
40
20
0
1.
2.
3.
Mo
Sr
Li
V
Cd
Mn
Cu
Zn
Al
Ba
Ni
Co
Pb
Cr
U
Fe
Ti

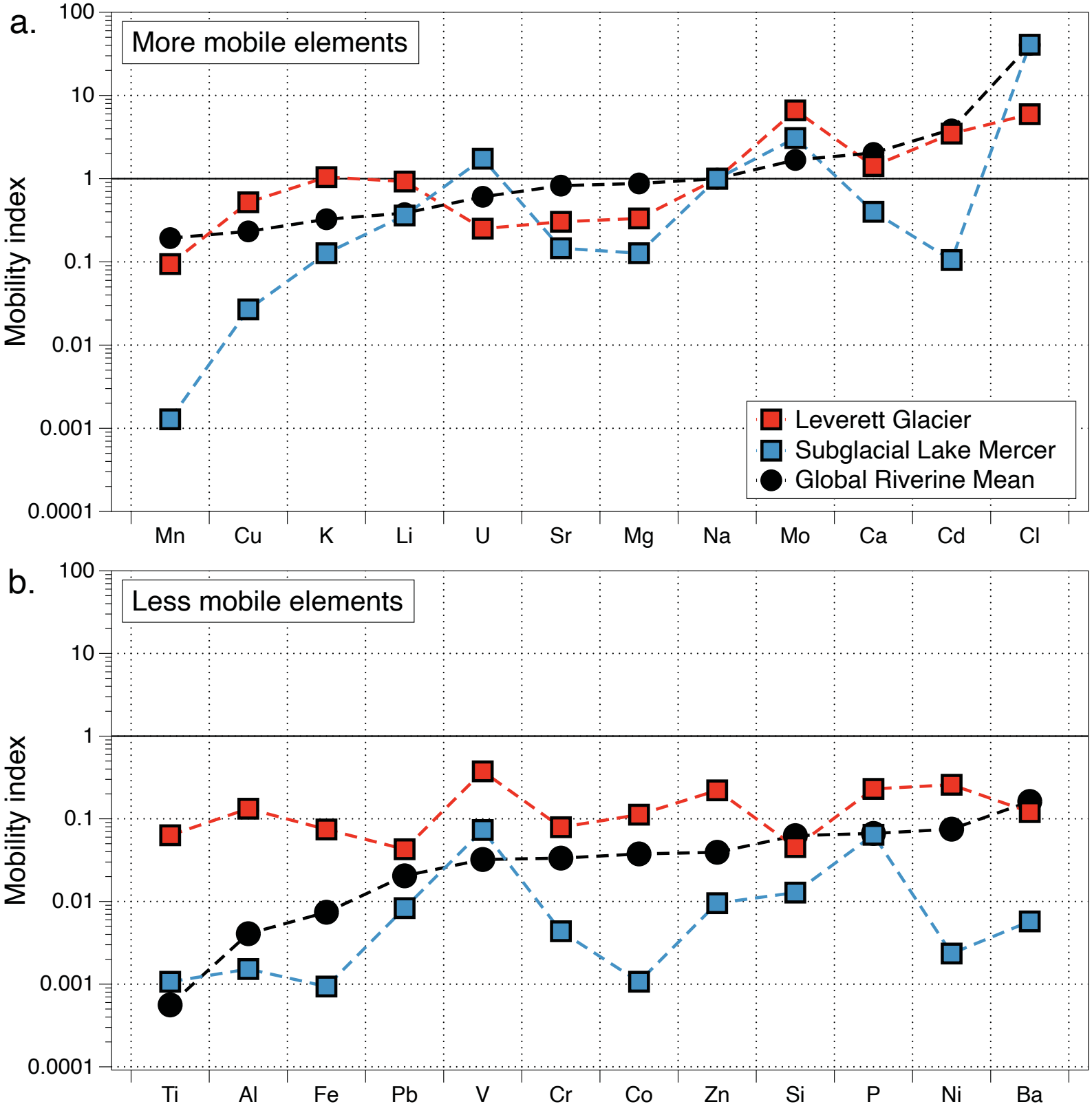
a.
More mobile elements
Mobility index
100
10
1
0.1
0.01
0.001
0.0001
Mn
Cu
K
Li
U
Sr
Mg
Na
Mo
Ca
Cd
Cl
Leverett Glacier
Subglacial Lake Mercer
Global Riverine Mean
b.
Less mobile elements
Mobility index
100
10
1
0.1
0.01
0.001
0.0001
Ti
Al
Fe
Pb
V
Cr
Co
Zn
Si
P
Ni
Ba